Cellular and Molecular Life Sciences (2023) 80:1
https://doi.org/10.1007/s00018-022-04645-z

ORIGINAL ARTICLE

RhoC in association with TET2/WDR5 regulates cancer stem cells by epigenetically modifying the expression of pluripotency genes

Pavana Thomas[1,2] · Sweta Srivastava[3] · Avinash H. Udayashankara[4] · Samyuktha Damodaran[1] · Lokendra Yadav[3] · Boby Mathew[5] · Srinag Bangalore Suresh[1] · Amit Kumar Mandal[5] · Nirmala Srikantia[4]

Received: 25 August 2022 / Revised: 22 November 2022 / Accepted: 22 November 2022 / Published online: 5 December 2022
© The Author(s), under exclusive licence to Springer Nature Switzerland AG 2022

Abstract

Emerging evidence illustrates that RhoC has divergent roles in cervical cancer progression where it controls epithelial to mesenchymal transition (EMT), migration, angiogenesis, invasion, tumor growth, and radiation response. Cancer stem cells (CSCs) are the primary cause of recurrence and metastasis and exhibit all of the above phenotypes. It, therefore, becomes imperative to understand if RhoC regulates CSCs in cervical cancer. In this study, cell lines and clinical specimen-based findings demonstrate that RhoC regulates tumor phenotypes such as clonogenicity and anoikis resistance. Accordingly, inhibition of RhoC abrogated these phenotypes. RNA-seq analysis revealed that RhoC over-expression resulted in up-regulation of 27% of the transcriptome. Further, the Infinium MethylationEPIC array showed that RhoC over-expressing cells had a demethylated genome. Studies divulged that RhoC via TET2 signaling regulated the demethylation of the genome. Further investigations comprising ChIP-seq, reporter assays, and mass spectrometry revealed that RhoC associates with WDR5 in the nucleus and regulates the expression of pluripotency genes such as Nanog. Interestingly, clinical specimen-based investigations revealed the existence of a subset of tumor cells marked by $RhoC^{+}/Nanog^{+}$ expression. Finally, combinatorial inhibition (in vitro) of RhoC and its partners (WDR5 and TET2) resulted in increased sensitization of clinical specimen-derived cells to radiation. These findings collectively reveal a novel role for nuclear RhoC in the epigenetic regulation of Nanog and identify RhoC as a regulator of CSCs. The study nominates RhoC and associated signaling pathways as therapeutic targets.

Keywords Radiosensitization · Self-renewal · Infinium MethylationEPIC array · ChIP-seq · Molecular drug targets

Introduction

According to the Globocan 2020 report, cervical cancer is the 4th most common cancer amongst women worldwide, while it is ranked 3rd in incidence and 2nd in mortality in India. Further, 90% of the incidences and deaths due to the disease occurred in low- and middle-income countries [1]. As per data from the American Cancer Society, the 5-year survival rate for the distant SEER (Surveillance, Epidemiology and End Results) stage of cervical cancer is 18%, while all the SEER stages combined present a 5-year survival rate of 66%. Patients in the localized SEER stage perform considerably better at a 92% survival rate. Though concurrent chemoradiation (CCRT) is the standard of care in stages Ib2 to IVa, it has its limitations concerning the size of the tumor [2, 3]. Thus, patients with metastases or therapy-resistant tumors exhibit poor prognoses.

Studies show that cancer stem cells (CSCs) drive therapy resistance, tumor heterogeneity, and metastasis [4]. These

✉ Sweta Srivastava
sweta.s@stjohns.in

1 Translational and Molecular Biology Laboratory (TMBL), Division of Molecular Biology and Genetics, St. John's Research Institute (SJRI), St. John's Medical College, Bangalore 560034, India

2 School of Integrative Health Sciences, The University of Trans-Disciplinary Health Sciences and Technology (TDU), Bangalore 560064, India

3 Translational and Molecular Biology Laboratory (TMBL), Division of Molecular Biology and Genetics, St. John's Medical College Hospital, Bangalore 560034, India

4 Department of Radiation Oncology, St John's Medical College Hospital, Bangalore 560034, India

5 Clinical Proteomics Unit, Division of Molecular Medicine, St. John's Research Institute (SJRI), St. John's Medical College, Bangalore 560034, India

cells possess self-renewal ability akin to normal adult stem cells and promote malignant growth, therapy resistance, and metastasis [5]. Eradication of CSCs would therefore be an ideal strategy to improve clinical outcomes. However, targeting CSCs has proved to be an onerous task as they possess highly efficient DNA repair and drug efflux abilities, analogous to adult stem cells [6]. Therefore, understanding their unique molecular landscape and identifying molecular targets have gained prime importance in the quest to eradicate CSCs. RhoC is one such signaling pathway that has been implicated in both metastases and therapy response [7].

RhoC is a member of the RhoGTPase family of proteins and regulates cell physiology, including actin organization and motility [8]. Subsequent studies also show its role in tumor progression. Significantly, a DNA array study on metastatic melanoma revealed that RhoC was essential for metastasis [9]. Another group discovered that while RhoC was indispensable for metastasis, it was not essential for normal embryogenesis in murine models [10]. Reports also suggest its role in an array of tumor hallmarks, such as EMT, metastasis and therapy resistance, across several types of cancers [11, 12]. RhoC-mediated alteration of the Mitogen-Activated Protein Kinase (MAPK) and Phosphoinositide 3-kinase/AKT Serine Threonine Kinase (PI3K/AKT) pathways is known to promote invasion [13, 14]. Regulation of angiogenesis by RhoC via VEGF, bFGF and interleukins has been reported in breast, cervical and oesophageal cancers [12, 15, 16]. Our earlier report shows that RhoC regulates DNA repair via ROCK2 signaling [11]. These findings highlight the essential role of RhoC in metastasis and therapy resistance.

Based on these findings, it is reasonable to postulate that RhoC may be an essential factor in CSC maintenance. Indeed, observations from Islam et al., and Rosenthal et al., demonstrate that RhoC regulates CSCs in head and neck and breast cancers [17, 18]. However, there is a lack of data to suggest its mechanism of action in this context. Additionally, there is no evidence thus far to support its role in cervical CSC maintenance. This study explores the role of RhoC in the maintenance of cervical CSCs and delineates the molecular mechanism of its action.

Our results confirm that RhoC plays a critical role in cervical CSC maintenance. We report a novel interaction between RhoC and the WDR5-MLL complex, which results in epigenetic regulation of pluripotency genes, such as Nanog. Radiation resistance is an impediment, and the lack of biomarkers to predict therapy response in cervical cancer amplifies the prevailing conundrum. Our work here provides evidence to confirm that RhoC could serve as an effective therapeutic target for cervical CSC sensitization.

Materials and methods

Cells lines and reagents

This study used SiHa, CaSki (squamous cervical carcinoma cell lines), HCT 116 (a colorectal cancer cell line), and PC-3 (a prostate cancer cell line) cell lines. While SiHa cells originate from primary cervical carcinoma, CaSki is a cell line derived from metastatic cervical lesions. DMEM was used to culture SiHa and CaSki cells, HCT 116 was cultured in McCoy's media, and PC-3 was cultured in RPMI media. The media contained 10% FBS and penicillin–streptomycin (15140148). The cultures were tested for mycoplasma contamination regularly. The Ambion siRNAs used for transfection were scrambled negative control (SCR) (AM4611), RhoC (120759, 120897), TET2 (126964), and WDR5 (136959). Table S1 is a list of all the primary antibodies used in this study. Secondary antibodies used were anti-mouse HRP (12-349), anti-rabbit HRP (12-348), Alexa 488 (A11034), Alexa 546 (A11030), and Alexa 647 (A21236). The live-dead assay utilized propidium iodide (P1304MP) (for dead cells) and Annexin V-FITC (556419) (for the apoptotic pool), while the dye-exclusion assay used Hoechst 33342 (H21492). Bobcat339 hydrochloride (S6682) and OICR-9429 (S7833) were used to inhibit TET2 and WDR5, respectively.

Processing of tumor biopsies

The biopsies were collected in PBS and dissociated into single cells [11]. Briefly, the specimen was minced into tiny pieces using a scalpel and forceps. The minced tissue was collected and subjected to enzymatic digestion using collagenase type IV (1 mg/ml). If required, the cells were incubated in 1X RBC lysis buffer on ice for 10 min, followed by a wash with 1X PBS to yield a clear white pellet. The single cells thus obtained were used for further experiments.

WST analysis

Cells were cultured in a 96-well plate (2000 cells/well) and treated with the appropriate chemical. Post-treatment, 10 µl WST-1 reagent (5015944001) was added and incubated at 37°C, 5%CO_2 for 30 min. A microplate reader was used to take OD readings at 450 nm with a background subtraction of 655 nm.

Treatment and irradiation of cells derived from tumor biopsies

The antibody inhibition method was employed to inhibit RhoC in biopsy-derived cells [11]. Briefly, saponin was

added to the media at a final concentration of 0.0025% (w/v). The RhoC antibody (SC-26481) was added to the media at a final concentration of 1 µg/ml and incubated for 48 h before radiation. Inhibitors for WDR5 (OICR-9429) and TET2 (BC-339) were used at concentrations of 10 µM (24 h) and 100 µM (72 h), respectively. The cells were then irradiated at 6 Gy and analyzed for apoptosis by FACS.

Flow cytometry for cell survival

Cells were washed once with 1XPBS after removal of media and detached using 5 mM EDTA. The cells were resuspended in 1X annexin binding buffer containing annexin (3:100) and incubated in the dark for 30 min. The cells were washed twice and resuspended in 1 ml of annexin binding buffer. Propidium iodide was added 2–3 min before analysis at a final concentration of 1 µg/ml. The cells were analyzed using the FC500 analyzer from Beckman Coulter.

Flow cytometry for immunostaining

Cells were washed once with 1XPBS after removal of media and detached using 5 mM EDTA. The cells were fixed in 1% paraformaldehyde (PFA) (w/v) for 5 min at room temperature and washed thrice in 1XPBS to remove excess PFA. Cells were permeabilized using 0.1% tritonX100 (v/v) in 1XPBS, and blocked using a cocktail of 5% FBS (v/v) and 2% BSA (w/v) in 1XPBS. The cells were then incubated in primary antibody (made in blocking reagent) at the appropriate dilutions at room temperature for 2 h. They were washed thrice in 1XPBS and incubated with a secondary antibody (made in 1XPBS) at the appropriate dilutions for 45 min at room temperature. The stained cells were washed thrice in 1XPBS and analyzed using FC500 or BD FACS Aria III.

Immunofluorescent staining for biopsy sections

The cryosections were washed once in 1XPBS followed by heat-fixation overnight at 55 °C. The slides were incubated in 0.01 M citrate buffer at 90 °C for 20 min for antigen retrieval. Once they cooled down to room temperature, the sections were permeabilized with 0.1% tritonX100 (v/v), blocked with 3% BSA (w/v), and washed thrice in 1XPBS. The primary antibody (made in blocking reagent) was added at the appropriate dilutions and incubated at room temperature for 2 h, followed by three 1XPBS washes and incubation with a secondary antibody (made in 1XPBS) for 45 min at room temperature. The nuclei were stained using DAPI (1 µg/ml), and the slides were mounted with VECTASHIELD anti-fade mounting media, followed by imaging using the Zeiss 710 confocal microscope. ImageJ software was used for image analysis. Colocalized pixels were analyzed using the Coloc2 and Colocalization threshold plugins available in the Image J software. The Manders score, Pearson's correlation coefficient, R, and the Costes P-value determined the extent of colocalization.

Immunofluorescent staining for cell lines

Cells were fixed in 1% PFA (w/v) for 5 min at room temperature and washed thrice with 1XPBS before staining. The cells were permeabilized using 0.1% tritonX100 (v/v) for 5 min and blocked using 0.2% fish skin gelatin (v/v) for 20 min at room temperature. Primary antibodies were added at the appropriate dilutions (in blocking reagent) and incubated at room temperature for 2 h. The cells were washed thrice with 1XPBS and secondary antibodies were added at the required dilutions (in 1XPBS) and incubated at room temperature for 45 min. The cells were washed thrice with 1XPBS, stained with DAPI (1 µg/ml) and mounted using VECTASHIELD anti-fade mounting media. Imaging and image analysis was done using the Zeiss 710 confocal microscope and ImageJ, respectively. Colocalized pixels were analyzed using the Coloc2 and Colocalization threshold plugins available in the Image J software. The Manders score, Pearson's correlation coefficient, *R*, and the Costes *P* value determined the extent of colocalization.

Clonogenic assay

For the clonogenic assay, 1000 cells were seeded in 100 mm dishes in DMEM supplemented with 10% FBS. The colonies formed were allowed to grow over 14 days. They were then stained with 0.05% crystal violet for 1 min, washed thrice with 1XPBS, and the colonies were counted.

Soft agar assay

5000 cells were seeded in 0.33% agar containing DMEM over a layer of 0.5% agar with DMEM and FBS in a 35 mm dish [12]. Media supplementation (200 µl) was done every 72 h. At the end of 21 days, the Leica DMIL LED Fluorescence microscope was used to count and image colonies.

Tumor sphere cultures

Culture of cells as spheroids used DMEM-F12 media supplemented with 20 ng/ml EGF and 10 ng/ml bFGF. 0.1 million cells seeded in 6-well plates coated with poly-hydroxyethyl methacrylate were allowed to grow, and spheroids formed counted at the end of 7 days from 10 random fields.

Limiting dilution assay

Serially diluted cells (to obtain a cell concentration of 100 cells/well and 10 cells/well in a poly-hydroxyethyl

methacrylate-coated 96-well plate) were seeded in DMEM-F12 media supplemented with 20 ng/ml EGF and 10 ng/ml bFGF. Microscopic visualization determined the presence of spheres.

Anoikis assay

0.1 million cells were seeded in 6-well plates coated with poly-hydroxyethyl methacrylate using DMEM devoid of FBS and cultured overnight. The following day, cell death analysis using flow cytometry was performed by annexin-V and propidium iodide staining.

Real-time quantitative PCR

RNA isolation was as described in the TRIzol method (Life Technologies, Invitrogen). Conversion of mRNA to cDNA used M-MLV reverse transcriptase (Life Technologies, Invitrogen), and gene expression studies by qPCR utilized the TB Green Premix Ex Taq II (RR820A, Takara). The 7500 Fast Real-Time PCR machine from ABI generated the Ct values which were used to calculate fold changes in gene expression. Table S2 contains the sequences of the primers used.

Western blotting

Cells were washed once with cold 1XPBS, incubated with lysis buffer (50 mM Tris HCl (pH7.4), 150 mM NaCl, 1% Triton X100, 2 mM EDTA (pH8.0), 0.1% SDS, 100 mM NaF, 200 mM Na3VO4, 10X MPI, 200 mM PMSF) for 30 min on ice, homogenized with an insulin syringe and centrifuged at 14,000 rpm for 10 min at 4 °C. The lysate was quantified using the BCA assay, and equal amounts of protein were loaded on an acrylamide gel and resolved using SDS-PAGE. The proteins were transferred onto a nitrocellulose membrane, blocked using 3% BSA (w/v) in 1XTBST and probed using the appropriate primary antibodies (made in the blocking reagent) at the required dilutions overnight at 4°C. The membranes were then washed thrice in 1XTBST and incubated with HRP-conjugated secondary antibodies for 1 h at room temperature. The membranes were washed thrice in 1XTBST, and the blots were imaged after ECL addition using the ChemiDoc XRS + system from BioRad.

Immunoprecipitation from nuclear proteins

Cells were washed with cold 1XPBS and cross-linked using 5 mM dithiobis-succinimidyl propionate (DSP) dissolved in 1% DMSO in 1XPBS. Post-incubation at room temperature for 30 min, 20 mM tris (pH 7.4) quenched the excess DSP. The cytosolic components were removed by incubating the cells with low osmotic buffer (50 mM Tris, 0.25% tritonX100, 100 mM NaCl, 10% glycerol, 5 mM EDTA, and MPI cocktail) for 10 min on ice. The nuclei were washed gently with cold 1XPBS and then incubated with NP-40 lysis buffer (50 mM Tris HCl (pH7.4), 150 mM NaCl, 2 mM EDTA (pH8.0), 1% NP-40, 100 mM NaF, 200 mM Na3VO4, 10X MPI, 200 mM PMSF). The nuclear fraction (NF) thus obtained was pre-cleared using Protein G dynabeads equilibrated with NP-40 lysis buffer. The dynabeads were incubated with the desired antibody at room temperature for 10 min and then added to the pre-cleared lysate. The proteins were allowed to bind overnight under gentle agitation at 4°C. The beads were washed and resuspended in 2X Laemmli buffer and incubated at 95°C for 10 min. The clear supernatant was subjected to immunoblotting.

2D gel electrophoresis and mass spectrometry

Immunoprecipitated proteins were subjected to isoelectric focusing using the Ettan IPGphor3 system from GE Healthcare. The IPG strips were then loaded onto an acrylamide gel and allowed to separate based on molecular weight. Post-silver staining, the unique spots were excised and de-stained in a wash solution (50% acetonitrile and 50 mM ammonium bicarbonate). Acetonitrile dehydrated the gel pieces, while a reduction solution (10 mM DTT and 100 mM ammonium bicarbonate) rehydrated them. The gel was treated with an alkylation solution (50 mM iodoacetamide and 100 mM ammonium bicarbonate). Post-washing, trypsin digestion was done, and the extracted peptides were subjected to MS/MS using the Bruker Daltonics ESI Q-TOF system with the Proxeon EASY-nLC. The data generated were analyzed using the MASCOT database to identify the precipitated proteins.

DNA Isolation and *Hpa*II digestion

DNA isolation by salting out helped extract DNA from cells. Here, cells were lysed using 600 µl cell lysis buffer and incubated with proteinase K (final concentration of 50 µg/ml) at 55°C for 3 h. The addition of 200 µl of 5 M potassium acetate and spinning at 14,000 rpm for 3 min helped precipitate proteins. 600 µl cold isopropanol precipitated DNA from the supernatant. After two ethanol washes and the dissolution of the DNA in nuclease-free water, quantification by the Qubit assay determined the concentration of DNA obtained [19]. 1 µg of the DNA was incubated with 5 units of the *Hpa*II enzyme (R0171S) at 37°C for 1 h. Densitometry was performed using the ImageJ software.

RNA-sequencing and analysis

The NEBNext Ultra Directional RNA Library Prep kit (E7420L) was utilized for RNA extraction and RNA-seq library preparation. RNA was sequenced using the Illumina

HiSeq paired-end sequencing (150×2). The raw data generated was checked for quality using FastQC and pre-processed, which includes removing the adapter sequences and the low-quality bases. Pre-processing of the data was done with the ABLT proprietary script. The reference genome used was the Homo sapiens DRCh38 build genome downloaded from the Ensemble database. Tophat-2.0.13 aligned the transcript sequences, and Cufflinks-2.2.1 performed assembly and differential expression. Cuffmerge created a combined assembly, while the Cuffdiff package performed Differential Gene Expression (DGE) analysis. Cut-off values of fold-change of 1.5 and 1/1.5 were used for up-regulation and down-regulation respectively. DAVID enabled gene Ontology (GO) analysis, while Heatmapper, a freely available web server, performed expression-based heatmap analysis [20]. The RNA-seq was in replicates of $n=2$. STRING database (version 11.0) was used to study the interaction networks [21], and the Shiny tool generated volcano plots.

Infinium human MethylationEPIC array and analysis

400 ng of good quality gDNA was subjected to bisulfite conversion using the EZ DNA Methylation kit (Zymo Research, D5002). The samples were then denatured and neutralized to prepare them for amplification using the Illumina Infinium Epic kit (WG-317-1002). Isothermal amplification of the denatured DNA was followed by fragmentation and precipitation by isopropanol. The precipitated DNA was resuspended in Hybridization Buffer and denatured at 95°C before loading onto the BeadChips. BeadChips were incubated for 18 h at 48°C for probe hybridization. Post-washes to remove unhybridized DNA, the BeadChips were scanned using Illumina iScan System to record high-resolution images of the light emitted from the fluorophores. RnBeads was used to combine the data into a RnBSet which stored DNA methylation levels as beta values. Quality control checks were carried out using minfi, ChAMP & RnBeads. The data was pre-processed by discarding CpGs that contain a substantial fraction with low technical quality and measurements that may be unreliable for other reasons. The normalization was performed using SWAN, and RnBeads was utilized to visualize the DNA methylation profiles. *P* values were calculated by the *limma* package and corrected for multiple testing using the FDR method. Strongly differentially methylated regions with a false discovery rate of <0.05 were taken for further analysis. Heatmaps for differential methylation were generated using the Heatmapper server, utilizing the individual *M* values of each replicate. *M* value is the log2 ratio of the intensities of the methylated versus the unmethylated probe. Sites with positive *M* values are hypermethylated, while those with negative *M* values are considered hypomethylated.

Chromatin immunoprecipitation

ChIP was performed using the Simple ChIP Enzymatic Chromatin IP Kit (CST 9003S) as per the manufacturer's protocol. Briefly, proteins were cross-linked to the DNA by adding PFA to the media at a final concentration of 4% (w/v). Excess PFA was quenched using glycine. The cells were washed twice with cold 1XPBS and collected in 2 ml of ice cold 1XPBS by scraping. The DNA from these cells was fragmented using both micrococcal nuclease and sonication. The cross-linked chromatin samples were treated with RNase A, and DNA was purified using the column method. The DNA was then quantified, and equal amounts of DNA were incubated with magnetic beads and the desired antibody overnight at 4°C. The beads were then washed thrice with high salt buffer, the DNA bound to the beads was collected using elution buffer, and the cross-links reversed using sodium chloride and proteinase K. The pulled-down DNA was purified using the column method and quantified using the DNA Qubit High sensitivity assay kit (Life Technologies, Invitrogen). Equal amounts of input DNA, DNA pulled down by the isotype control (IgG), and DNA pulled down by specific antibodies were tested for promoter enrichment by qPCR analysis. Values were normalized against the isotype (IgG) control.

ChIP sequencing and analysis

Libraries were prepared using the NEB Next Ultra II DNA Library preparation kit. In brief, ChIP DNA was subjected to various enzymatic steps for repairing the ends and attaching the dA-tail. After adapter ligation, fragments were then size-selected using SPRI beads. Next, the size-selected fragments were indexed during limited cycle PCR to generate final libraries for paired-end sequencing. Illumina HiSeq X Ten system quantified and sequenced the resulting libraries to generate 2X50 bp sequence reads. Post-quality checks, the paired-end reads were aligned to the reference human genome Feb. 2009 release downloaded from the UCSC database (GRCh37/hg19). Alignment was performed using BWA MEM (Ver-0.7.12). Model-based analysis of ChIP-Seq (MACS 2.1.3 version) carried out the peak calling analysis and identification of the statistically significant peaks. The resulting files were analyzed using the MEME suite to identify the enriched motifs [20].

Luciferase assay

Nanog promoter activity was assayed using the Dual-Luciferase Reporter Assay System from Promega (E1910) as per the manufacturer's protocol. Cells under various treatment conditions were transfected with the pNanog-Luc plasmid procured from Addgene (25900) and Renilla-Luc. Post-cell

lysis, the LUMI luminometer from MicroDigital recorded the readings. The readings thus obtained were normalized against the respective experimental controls.

Statistical analysis

The mean and standard deviations were computed for the experiments performed in triplicates. The significance of the difference between the test and control samples was calculated using the *t* test for groups of two. *P* values of less than 0.05 were considered significant.

Results

RhoC regulates the expression of stemness genes in cervical carcinoma cell lines

Since RhoC has been reported to regulate metastasis, EMT, tumor growth, angiogenesis, invasion, migration and therapy response in several tumors [7], including cancer of the cervix [12], it may be considered as an essential regulator of tumor progression. Since CSCs exhibit all of the above phenotypes, RhoC may be crucial in CSC maintenance. While there are reports of RhoC regulating CSCs in head and neck, and breast cancers [17, 18], there is a lack of data suggesting a similar parallel role in cervical cancer. Further, its mechanism of action in this context remains obscure. Thus, discerning the contribution of RhoC in cervical CSC maintenance and understanding its precise mode of action will be of immense translational significance.

CSCs have enhanced stem-like ability and expression of pluripotency-associated genes. Thus, molecular and phenotypic studies were conducted to assess the contribution of RhoC in the regulation of expression of stemness genes in the cervical carcinoma-derived cell line, SiHa. Previously published RNA-seq analysis comparing the transcriptional status of SiHa-R (cells over-expressing RhoC) and SiHa-N (cells with the backbone vector alone) [11] was further analyzed to understand the effect of RhoC over-expression on stemness-associated genes. Validation, using western blot analysis, of the over-expression of RhoC in SiHa-R cells has been reported previously [11]. The evaluation of this RNA-seq data revealed the hypertranscriptional status of SiHa-R cells (Fig. 1A and B). A detailed gene ontology (GO) analysis using DAVID revealed that the over-expressed genes were involved in biological processes such as cell division, proliferation, cell cycling, stemness, and cell signaling, amongst many others (Fig. S1A). STRING analysis of the same gene set also exhibited the enrichment of similar biological activities (Fig. S2). Cytoplasmic component (CC) analysis showed that a large proportion of the up-regulated genes translated into proteins that were localized in the nuclear compartment (Fig. S1B). Further, in-depth analysis of the over-expressed genes identified an array of stemness-associated factors, such as AURKA, SMAD2, NfkB1, and POSTN, to be up-regulated in SiHa-R cells (Fig. 1C). Similarly, there was an enrichment of genes involved in epigenetic modifications (Fig. 1D). qPCR and western blotting experiments were done to validate the expression of some of these selected genes. As shown in Fig. 1E–H, there was increased expression of Nanog, Sox2, ABCG2, CD49f, ALDH, and other markers of stemness in SiHa-R cells. It was also found that the over-expression of constitutively active RhoC in SiHa cells (SiHa-CA) resulted in the enrichment of stemness markers (Fig. S1C).

Previously reported and validated siRNAs for RhoC [11, 12] were used to assess the effect of RhoC silencing on stemness gene expression, and the efficacy of RhoC knockdown was confirmed using western blot (Fig. S1D). As shown in Fig. 1I RhoC knockdown resulted in decreased levels of stemness genes such as Nanog, CD49f, ALDH, POSTN and Sox2, amongst others. Western blot analysis confirmed that the expression of Nanog, an important pluripotency gene, decreased upon RhoC knockdown (Fig. 1J and K). CD49f, an important marker of cervical CSCs [21], was also found to be significantly reduced upon RhoC knockdown (Fig. 1J and L). Our previous study showed that RhoC over-expression in SiHa cells resulted in the formation of significantly larger tumors as compared to SiHa-N cells [12]. Cryosections of these xenograft tumors were used in the present study to assess the expression of stemness genes in SiHa-R xenografts. Consistent with our above findings, immunofluorescent analysis of Nanog, CD49f and ALDH in SiHa-R and SiHa-N xenografts sections showed increased expression of these markers in SiHa-R (Fig. 1M and S1E). The mean fluorescence intensity for Nanog was 18.873 AU and 20.463 AU in SiHa-N and SiHa-R xenografts, respectively. Similarly, CD49f showed an increase in mean fluorescence intensity in SiHa-R xenografts (8.236 AU), compared to SiHa-N xenografts (5.671).

RhoC regulates stemness phenotype in cervical carcinoma cell lines

Given that RhoC impacts the expression of stemness genes, it was critical to determine its effect on stemness phenotypes such as self-renewal ability and anoikis resistance. Clonogenic, spheroid formation and soft agar assays were performed to assess the effect of RhoC expression on self-renewal ability. As shown in Fig. 2A and S1F, SiHa-R cells formed more clones when compared with SiHa-N cells. Similarly, soft agar assays also revealed that SiHa-R cells had an enhanced ability to form colonies as compared to SiHa-N cells (Fig. 2B and S1G). Clonogenic assay on SiHa-CA cells also demonstrated the enhanced clonogenicity of

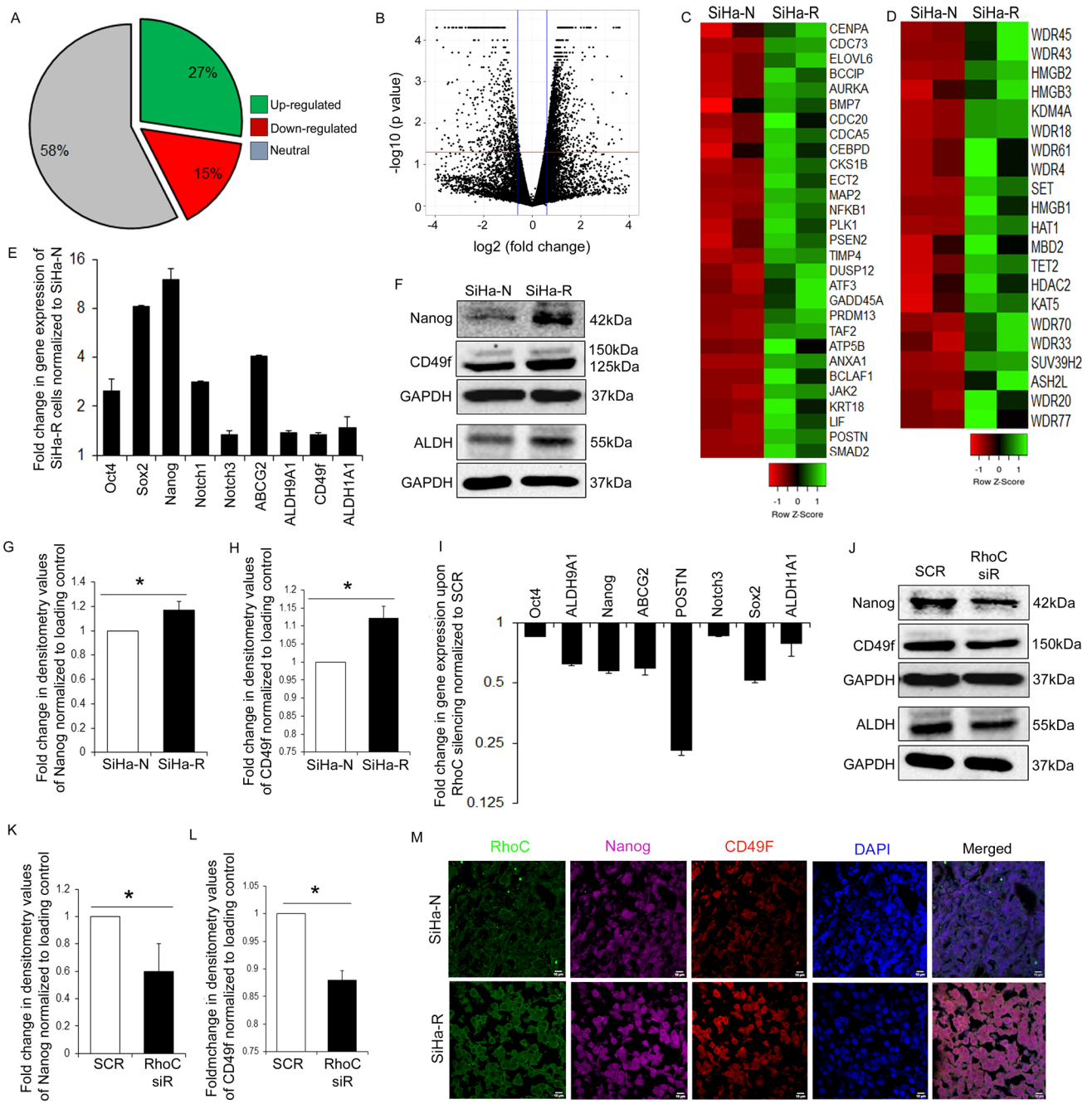

Fig. 1 RhoC over-expression results in a hypertranscriptional cell with enriched stemness signatures. **A** Pie-chart depicting up-regulation of 27% of the genes in SiHa-R cells as revealed by the RNA-seq data. **B** Volcano plot of genes in SiHa-R, displaying up-regulation of a majority of the genes. **C** An increase in expression of genes involved in stemness in SiHa-R was observed by analysis of RNA-seq data represented by a heatmap. **D** Heatmap representation of the up-regulated genes in SiHa-R known to be involved in epigenetic modifications. **E** qPCR analysis depicts up-regulation of genes regulating stemness in SiHa-R cells. Gene expression values were normalized to SiHa-N, using GAPDH as the internal control ($n=3$, $P<0.05$). **F** Immunoblotting confirms the enrichment of stemness signatures Nanog, CD49f and ALDH in SiHa-R cells ($n=3$). GAPDH was used as the loading control. Representative images are shown. Fold change in densitometry values of Nanog (**G**) and CD49f (**H**) in SiHa-R cells ($n=3$, $P<0.05$). **I** siRNA-mediated silencing of RhoC leads to decreased expression of stemness genes in SiHa cells as observed by qPCR analysis. Values were normalized to cells treated with scrambled negative control siRNA (SCR). GAPDH was used as the internal control ($n=3$, $P<0.05$). **J** A representative western blot image corroborating down-regulation of Nanog, CD49f and ALDH in cells knocked down for RhoC ($n=3$). Loading levels were verified using GAPDH. Fold change in densitometry values of Nanog (**K**) and CD49f (**L**) in SiHa cells knocked down for RhoC ($n=3$, $P<0.05$). **M** Immunofluorescent analysis of SiHa-N and SiHa-R xenograft sections shows an increase in Nanog and CD49f, along with RhoC, in SiHa-R xenografts (scale bars are indicated)

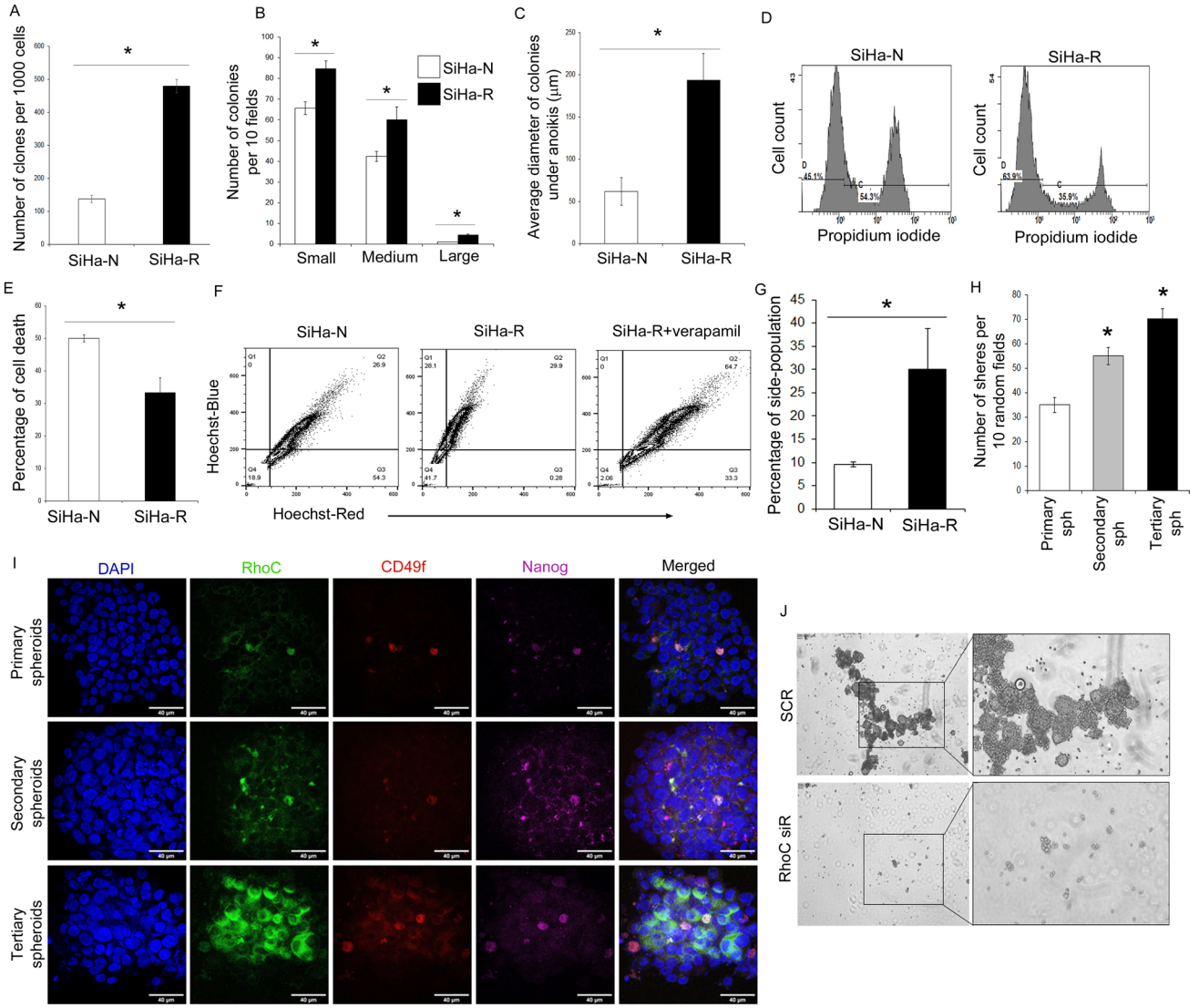

Fig. 2 RhoC endows cervical cancer cells with enhanced stem-like ability. **A** Bar graph representation of the average number of clones formed by SiHa-N and SiHa-R cells in the clonogenic assay, with SiHa-R cells displaying a clear advantage ($n=3$, $P<0.05$). **B** Bar graph representation of the numbers of small, medium and large colonies formed by SiHa-N and SiHa-R cells in the soft agar assay ($n=3$, $P<0.05$). **C** Graphical representation of the average diameter of aggregates formed under anoikis-inducing conditions, with SiHa-R cells forming significantly larger aggregates than SiHa-N ($n=3$, $P<0.05$). **D** Representative FACS plot showing the decreased percentage of cells stained for propidium iodide in SiHa-R when cultured under anoikis-inducing conditions. **E** Bar graph representing the average percentage of cell death seen under suspension in SiHa-N and SiHa-R cells ($n=3$, $P<0.05$). **F** Representative FACS plot depicting the superior efflux ability of SiHa-R cells as compared to the verapamil treated control. SiHa-R cells were observed to have a larger percentage of cells capable of effluxing the Hoechst dye (side-population). **G** Graphical representation of the average percentage of Hoechst negative cells (side-population) in SiHa-N and SiHa-R ($n=3$, $P<0.05$). **H** Graphical representation depicting increase in the number of spheroids upon serial passaging of SiHa cells over 10 random fields ($n=3$, $P<0.05$). **I** Representative images depicting co-expression of RhoC with CD49f and Nanog in serially passaged spheroids (n=3). Scale bars are indicated. **J** Representative images showing abrogation of sphere formation ability upon RhoC knockdown (n=3)

these cells, as shown in Fig. S1H and S1I. Conversely, the knockdown of RhoC using siRNA resulted in reduced clonogenic ability (Fig. S1J and S1K). Additionally, the effect of RhoC expression was also tested on anoikis resistance. In an anoikis assay, the SiHa-R cells formed larger aggregates (Fig. 2C and S1L), and survived better (Fig. 2D and E) when compared to the SiHa-N cells. Similarly, SiHa-CA cells also showed enhanced survival under anoikis-inducing conditions (Fig. S1M and S1N). Further, to confirm that RhoC expression modulates the stem-cell population, consequently regulating self-renewal ability as observed above, assays were performed using Hoechst 33342 to assess

side-population enrichment following RhoC over-expression. Over-expression of RhoC resulted in the enrichment of the side-population, and this pool of cells was depleted upon treatment with verapamil, a blocker of efflux activity (Fig. 2F and G). All the cells chosen for the analysis were live (Fig. S1O). Enhanced efflux of dyes is a vital CSC property [22], thus an increase in side-population observed due to RhoC over-expression indicated enrichment of CSCs. The tumor sphere assay measures the self-renewal ability of stem-like cells [23]. Serial passaging of SiHa tumor spheres showed a successive increase in the number of spheres with secondary and tertiary passages (Fig. 2H). Expression of stemness markers Nanog and CD49f also increased across the serial passage and was maximum in the tertiary spheres, as expected. Significantly, RhoC was co-expressed with Nanog and CD49f in these spheres, indicating a positive correlation between RhoC and increased stem-like ability (Fig. 2I). Concurrently, the knockdown of RhoC in SiHa cells resulted in no clones due to the complete abrogation of sphere-forming ability (Fig. 2J). The limiting dilution assay, another technique to determine stem-like ability [24], showed an increased clonogenic ability of SiHa-R cells even at minimal numbers of 10 and 100 cells per well of a 96-well plate (Fig. S1P). The siRNA treatment resulted in a complete knockdown thus no clones were formed.

CaSki, another cervical cancer cell line, was also used to confirm the role of RhoC in CSCs. The CaSki-dnR cells (CaSki cells stably over-expressing dominant negative RhoC) were less clonogenic as compared to CaSki-N (CaSki with pcDNA3 backbone vector) (Figs. S1Q and S1R). CaSki-dnR cells cultured under suspension conditions also formed smaller-sized aggregates as compared to CaSki-N (Figs. S1S and S1T).

Since CD49f's expression is regulated by RhoC, its knockdown resulted in reduced clonogenic ability of SiHa-R cells (Figs. S1U and S1V). Alternatively, its over-expression in CaSki-dnR resulted in a partial gain of clonogenic ability (Fig. S1W). Collectively, the above data suggest that RhoC transcriptionally up-regulates stemness genes resulting in the display of robust stemness phenotypes.

RhoC over-expressing cells have hypomethylated DNA, aiding hyper-transcription

Hypertranscriptional cells require open chromatin to enable transcriptional activities, and given that SiHa-R cells have a hypertranscriptional status, studies were performed to examine its chromatin [25–27]. Investigation of the chromatin status revealed that tumor cells with nuclear localization of RhoC presented with weak staining of DNA with DAPI (4′-6-diamidino-2-phenylindole) (Fig. S3A), a chemical that binds to the minor grooves of DNA and is routinely used to detect chromatin compactness [28]. The open chromatin observed in SiHa-R cells may be due to alterations in DNA methylation or histone modifications.

Hypomethylated DNA is associated with hyper-transcriptional activity and cancer progression [29]. In consonance with this, our observation using restriction endonuclease treatment of DNA by *Hpa*II, a methylation-sensitive restriction enzyme, showed extensive endonuclease activity in SiHa-R cells as compared to SiHa-N cells, implying hypomethylation of DNA in SiHa-R cells (Fig. S3B). Quantitative FACS analysis of SiHa-R cells revealed significantly lesser 5-methylcytosine (5mC, a marker of DNA methylation) in SiHa-R compared to SiHa-N (Fig. 3A and B). Further, siRNA mediated RhoC knockdown in SiHa cells caused an increase in 5mC levels (Fig. 3C and D). These findings were further validated using the Infinium Human Methylation 850k (EPIC array). A comparative analysis of SiHa-N and SiHa-R DNA revealed significant changes in DNA methylation upon RhoC over-expression (Fig. 3E), with 426 sites showing hypomethylation (differential methylation value of less than − 0.1), 328 displaying hypermethylation (differential methylation value of more than 0.1) and 2784 showing no significant change (differential methylation values between − 0.1 and 0.1) (Fig. 3F). Additionally, genes over-expressed in SiHa-R cells were found to have hypomethylated regions. The hypomethylation status of Sox2, ABCG8, Nanog and ABCG2 are shown in Fig. S3C, S3D, S3E and S3F. Fig. 3G, H and I, represent sites within various genes involved in stemness maintenance, signaling pathways and epigenetic alterations that were observed to be demethylated in SiHa-R. These data convincingly demonstrate that RhoC over-expressing cells have hypomethylated DNA, which may be linked with increased expression of stemness-associated genes.

RhoC regulates hypomethylation of DNA via TET2

In order to investigate how RhoC regulates DNA methylation, studies were planned to identify the role of RhoC in TET (ten-eleven translocation dioxygenases) enzyme regulation, which are known to be responsible for loss of DNA methylation [30]. Transcriptomic data showed a significant up-regulation of TET2 in SiHa-R cells (Fig. 4A), and this increased expression was also confirmed by immunofluorescent analysis (Fig. 4B). siRNA-mediated knockdown of RhoC led to decreased expression of TET2 in SiHa cells, with no change in the levels of TET1 and TET3 upon RhoC silencing (Fig. 4C and S3G).

The modulation of DNA methylation by TET2 in SiHa cells was confirmed by assessing the 5mC levels in SiHa cells knocked down for TET2. TET2 siRNA successfully silenced TET2 in SiHa cells (Fig. 4D) and increased levels of 5mC, reaffirming TET2's role in DNA hypomethylation (Fig. 4E and S3H). Additionally, TET2 silencing increased

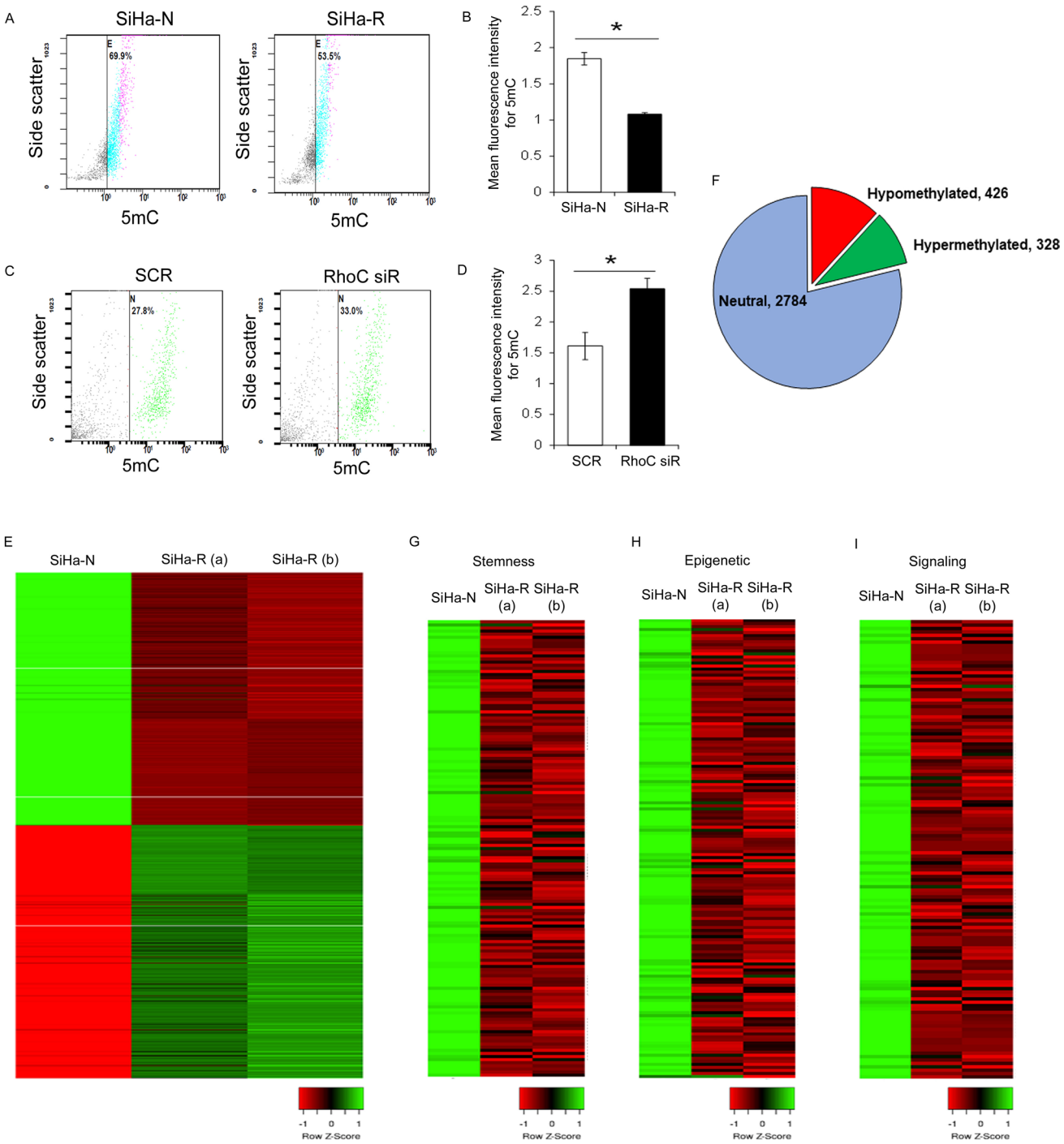

Fig. 3 RhoC leads to transcriptional up-regulation by causing global alterations in DNA methylation levels. **A** Representative FACS plot showing a decrease in 5mC levels in SiHa-R in comparison with SiHa-N ($n=3$). **B** Bar graph representation of mean fluorescence intensity (MFI) of 5mC in SiHa-N and SiHa-R ($n=3$, $P<0.05$). **C** Representative FACS plot showing increased 5mC upon siRNA-mediated RhoC knockdown in SiHa cells ($n=3$). **D** Bar graph representation of MFI of 5mC, showing an increase in 5mC levels upon RhoC knockdown (RhoC siR) in comparison with control cells (SCR) ($n=3$, $P<0.05$). **E** Heatmap representation of top differentially methylated sites in SiHa-N and SiHa-R cells. **F** Pie-chart depicting the distribution of methylation at various sites in the genome in SiHa-R cells. Heatmap representation of *M* values of various sites of genes associated with stemness (**G**), signaling (**H**) and epigenetic changes (**I**), previously found to be over-expressed in SiHa-R cells, showing decreased methylation values in SiHa-R

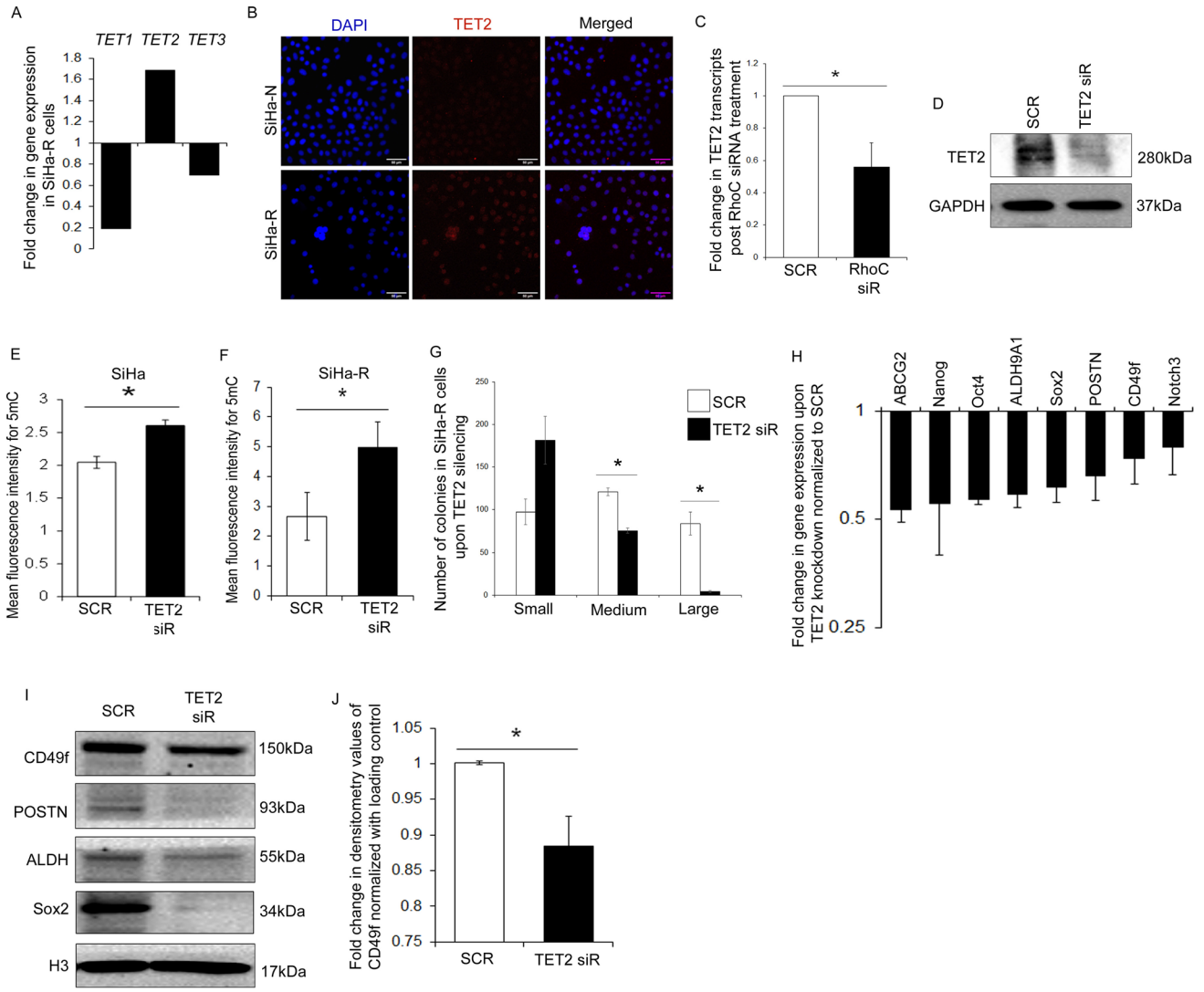

Fig. 4 RhoC via TET2, an active DNA demethylase, enhances stemness capability. **A** Bar graph showing a significant increase in TET2 transcripts, and not TET1 and TET3, in SiHa-R cells (normalized against SiHa-N), as revealed by the RNA-seq data. **B** Immunofluorescent analysis of TET2 confirms up-regulation in SiHa-R cells ($n=3$). (scale bars are indicated) **C** qPCR analysis depicts a decrease in TET2 mRNA levels upon siRNA-mediated RhoC knockdown (RhoC siR) in comparison with scrambled control (SCR) ($n=3$, $P<0.05$). GAPDH was used as the internal control. **D** Representative western blot image to show successful knockdown of TET2 upon transfection with TET2 siRNA ($n=3$). **E** Bar graph representation of increased MFI of 5mC in TET2 siRNA treated SiHa cells ($n=3$, $P<0.05$). **F** Bar graph representation of increased MFI of 5mC in SiHa-R cells knocked down for TET2 ($n=3$, $P<0.05$; *y*-axis in multiples of 1000). **G** Bar graph representation depicting the average number of colonies formed by SiHa-R cells upon TET2 silencing, showing that reduction in TET2 levels led to successful abrogation of the stemness advantage of SiHa-R cells ($n=3$, $P<0.05$). **H** Bar graph representation of transcript levels of stemness genes in SiHa-R cells upon TET2 knockdown ($n=3$, $P<0.05$). Values were normalized against the scrambled control (SCR), using AICDA as the internal control. **I** Immunoblotting confirms down-regulation of stemness genes in SiHa-R upon TET2 silencing ($n=3$). Representative images are shown. **J** Bar graph showing fold change in densitometry values of CD49f upon TET2 silencing ($n=3$, $P<0.05$)

5mC levels in SiHa-R cells, confirming its role in DNA demethylation in the background of RhoC (Fig. 4F). Importantly, the knockdown of TET2 mitigated the gain in the clonogenic and self-renewal ability of SiHa-R cells, with a specific loss in the ability to form large colonies (Figs. 4G and S3I). TET2 knockdown also reversed the expression of Nanog, Sox2, ALDH, POSTN, and CD49f in SiHa-R cells (Fig. 4H, I, J, S3J, S3K and S3L). These data show that the gain of phenotype due to RhoC over-expression is diminished upon TET2 silencing and TET2 phenocopies RhoC, suggesting that RhoC via TET2 mediates DNA demethylation consequently resulting in increased expression of stemness associated genes.

WDR5 is the nuclear interacting partner of RhoC

It is important to note that RhoC does not have a DNA-binding domain, so it must exert its nuclear activity through other proteins. Thus, investigations were performed to identify proteins that may interact with RhoC in the nuclear compartment. Immunoprecipitation of RhoC from the nuclear fraction (Fig. S4A) of SiHa-R cells, followed by 2D gel electrophoresis and mass spectral (MS) analysis of the unique spots obtained after silver staining (Fig. S4B), resulted in the identification of WDR5 as an interacting partner of RhoC (Fig. 5A). The observed interaction was further validated by performing RhoC and WDR5 immunoprecipitations, followed by the detection of WDR5 and RhoC, respectively, in the pulled-down complexes (Fig. 5B and C). To confirm these observations, confocal imaging was performed to determine the colocalization of RhoC and WDR5. There was significant colocalization between RhoC and WDR5 in SiHa-R cells (Fig. 5D) and clinical specimen cryosections (Fig. 5E). Colocalization analysis using the ImageJ software was used to generate colocalized pixel maps, with colocalized pixels indicated in white. Manders coefficients [31] associated with each image (M1 for red pixels and M2 for green pixels) were used to determine the extent of colocalization. The correlation coefficient R was found to be 0.43 in SiHa-R cells, and 0.34 in the biopsy-derived cryosections. The Costes P-value was found to be 1 for both cases, indicating that the colocalization observed was indeed true.

WDR5 is a SET1/COMPASS complex protein and has been associated with tumor progression in the breast cancer model [32]. To investigate if RhoC interacts with this complex, nuclear RhoC was immunoprecipitated, and MS analysis was performed on the entire complex. The MS data reconfirmed the existence of WDR5 (Fig. S4C) and also

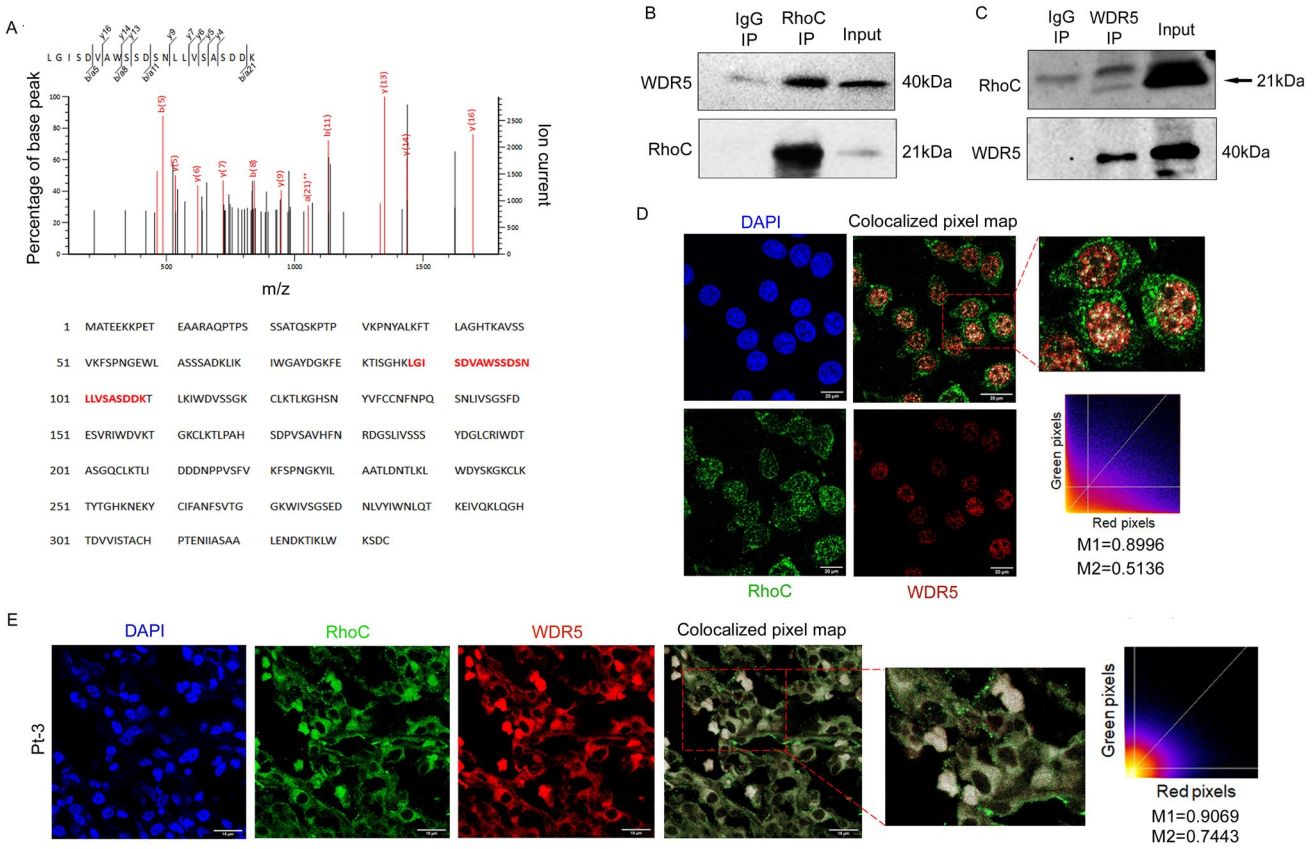

Fig. 5 RhoC interacts with WDR5, an epigenetic modifier, within the nuclei of cervical cancer cells. **A** Results of the mass spectrometry analysis with residues shown in red indicating an overlap with the amino acid sequence for WDR5. **B** Representative immunoblot image showing detection of WDR5 and RhoC in nuclear SiHa-R lysates pulled down with the RhoC antibody ($n=3$). **C** Representative immunoblot image showing positive detection of RhoC and WDR5 in nuclear lysates of SiHa-R upon WDR5 pull down ($n=3$). **D** Confocal imaging confirms the interaction of RhoC and WDR5 in SiHa-R cells ($n=3$). Representative images are shown. (scale bars are indicated). M1 and M2 are Manders coefficients of red pixels and green pixels respectively. The R value was found to be 0.43, while the Costes *P* value was found to be 1. **E** Representative immunofluorescent image showing co-localization of RhoC and WDR5 in a patient-derived tumor section (scale bars are indicated). M1 and M2 are Manders coefficients of red pixels and green pixels respectively. The *R* value was found to be 0.34, while the Costes *P* value was found to be 1

detected the presence of MLL1, another important component of the SET complex (Fig. S4D). Further, immunoprecipitation and western blotting confirmed that RhoC indeed interacts with MLL1 (Fig. S4E), with RhoC immunoprecipitation resulting in the isolation of MLL1. Concurrently, immunoprecipitation of MLL1 resulted in the isolation of RhoC (Fig. S4F). These observations confirm that RhoC co-operates with the MLL-WDR complex and regulates transcription via this complex.

WDR5 and RhoC co-operate to regulate stemness in SiHa cells

H3K4 is a downstream substrate of WDR5 [33], thus, studies were performed to determine the regulation of H3K4 by WDR5 in SiHa cells. As expected, WDR5 knockdown results in decreased H3K4me3 levels, as shown in Fig. 6A. Since RhoC and WDR5 interact, disruption of this association by knocking down either RhoC or WDR5 should result in reduced H3K4me3 levels. Indeed, RhoC siRNA transfection showed a marked reduction in H3K4me3 levels compared to control cells (Fig. 6B). Similarly, WDR5 knockdown in SiHa-R cells resulted in decreased nuclear H3K4me3 levels (Fig. 6C).

Phenotypic assays revealed that WDR5 knockdown abrogated RhoC-mediated gain in the clonogenic ability of SiHa cells. Upon WDR5 knockdown (Figs. S4G and S4H), the SiHa-R cells formed lesser colonies (Fig. 6D and S4I). Expression analysis of Nanog, Sox2 and ALDH revealed that WDR5 knockdown in SiHa-R cells mitigated the increase in expression of stemness genes observed due to RhoC over-expression (Fig. 6E, F and G). The transcriptional regulation of Nanog by RhoC and WDR5 was further validated using a luciferase-based reporter assay for Nanog. As expected, transient over-expression of RhoC (wtR) resulted in increased Nanog promoter activity in comparison with the backbone vector alone (pcDNA3) (Fig. 6H). Conversely, the knockdown of RhoC and WDR5 in SiHa cells resulted in a partial but significant decrease in the activity of the Nanog promoter (Fig. 6I and J), thus supporting the finding that the RhoC-WDR5 complex regulates the transcription of Nanog. To further confirm that RhoC and WDR5 regulate the expression of pluripotency-associated genes, a ChIP-sequencing experiment was performed. Analysis of ChIP-sequencing data showed that the occupancy profiles of RhoC and WDR5 on the genomic DNA were similar (Fig. 7A and B). STREME tool, from the MEME suite, was used to identify motifs to which RhoC and WDR5 bind [34]. Identified motifs were compared against the Human DNA database using the TOMTOM tool [35]. The RhoC ChIP-sequencing reads yielded 16 established motifs, while WDR5 yielded 12 motifs. TOMTOM-based analysis revealed that the 16 motifs identified by RhoC ChIP-seq were present on 172 genes, while the 12 motifs identified by WDR5 ChIP-seq matched with 148 genes. The genes identified following TOMTOM were analyzed using Interactivenn to identify commonly occupied motifs [36]. Interestingly, RhoC and WDR5 occupied common promoter regions of 106 genes (Fig. 7C and Table S3). The common genes identified in the RhoC and WDR5 ChIP seq were analyzed using STRING to determine specific clusters and associated networks regulated by them [21]. STRING analysis revealed the presence of four overlapping networks (Fig. S5A). Biological process (BP) analysis revealed that many of the identified genes were involved in transcriptional regulation and developmental processes, in line with our hypothesis that RhoC results in a hyper-transcriptional cell (Fig. 7D). Molecular function (MF) analysis indicated that the genes occupied by RhoC and WDR5 had DNA binding and transcriptional factor activity, further validating our claim (Fig. 7E and S5B). Reactome analysis of the 106 genes whose promoter regions are occupied by both RhoC and Nanog, revealed the possible pathways that these genes regulate [37], wherein 57 out of 106 genes were found in the Reactome database, and 308 pathways were hit by at least one of them. A genome-wide overview suggested that the enriched genes were associated with immune response, developmental biological processes, signal transduction and gene expression, with the most significant pathways being nuclear receptor transcription, developmental biology and transcriptional regulation of pluripotency genes (Figs. S5C, S5D and S5E). DAVID, STRING and Reactome analyses indicate that the genes occupied by both RhoC and WDR5 are involved in pluripotency maintenance and transcriptional processes. Stemchecker analysis was then performed on the 106 genes [38] to distinguish the stemness-associated genes. The analysis revealed that the genes enriched by RhoC and WDR5 were part of the expression profiles predominant in iPSCs, embryonal carcinoma, ESCs, neural SCs, HSCs and mammary SCs (Fig. 7F and G). These findings elucidate that the genes/genome sequences occupied by RhoC and WDR5 have a significant contribution to transcriptional regulation and stemness maintenance.

The ChIP-seq data also revealed the enrichment of motifs specific to the Nanog promoter, and that both RhoC and WDR5 enriched the same motif present in the Nanog promoter sequence (Fig. 7H and I). This data was further validated by qPCR of the RhoC and WDR5 ChIP DNA, with fold changes normalized against the isotype control. As shown in Fig. 7J, K and S5F, the Nanog promoter was enriched in both RhoC and WDR5 pull-downs. Cumulatively, the above data support the role of RhoC in the positive regulation of pluripotency-associated genes' expression in association with WDR5.

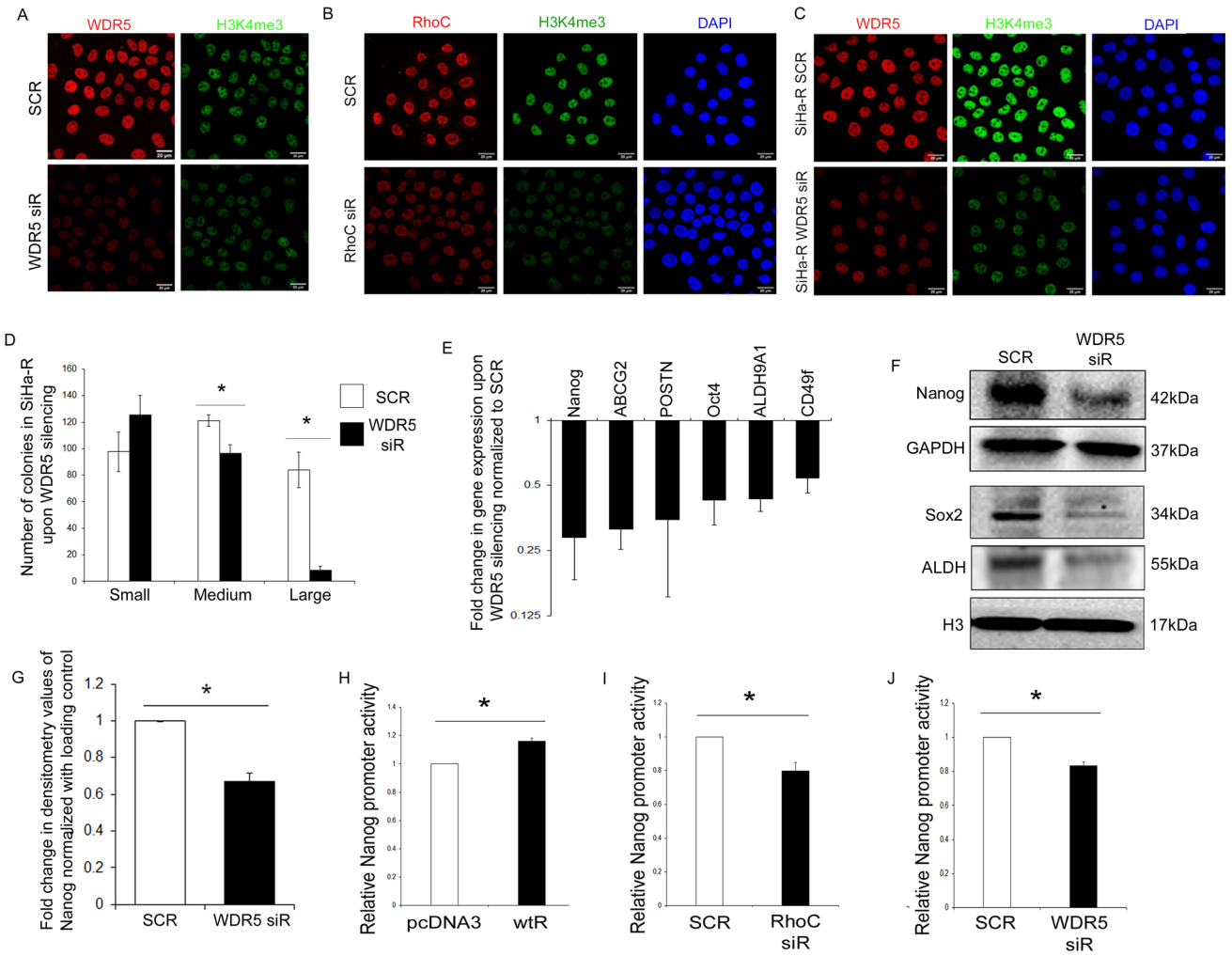

Fig. 6 RhoC and WDR5 alter H3K4me3 levels and regulate stem-like ability. **A** Knockdown of WDR5 in SiHa cells was seen to lead to successful reduction in H3K4me3 levels, as compared to the scrambled negative control (SCR) ($n=2$). Representative images are shown (scale bars are indicated). **B** siRNA-mediated silencing of RhoC resulted in a corresponding decrease in H3K4me3 levels as compared to scrambled control (SCR) ($n=2$). Representative images are shown (scale bars are indicated). **C** Representative image showing a reduction in WDR5 and consequent decrease in H3K4me3 levels in SiHa-R cells upon WDR5 knockdown ($n=2$) (scale bars are indicated). **D** Bar graph representation of the number of colonies formed by SiHa-R cells upon WDR5 siRNA treatment. WDR5 silencing was observed to result in loss of colony-forming ability in SiHa-R cells ($n=3$, $P<0.05$). **E** qPCR analysis depicts a reduction in mRNA levels of genes involved in stemness maintenance in SiHa-R cells knocked down for WDR5 ($n=3$, $P<0.05$). **F** Immunoblot analysis confirms a reduction in Nanog, Sox2 and ALDH upon WDR5 silencing, in comparison with scrambled control ($n=3$). Representative images are shown. **G** Bar graph showing fold change in densitometry values of Nanog upon WDR5 silencing ($n=3$, $P<0.05$). **H** Bar graph representation of the increase in Nanog promoter activity upon transient transfection of the RhoC-overexpressing plasmid (wtR) in comparison with the backbone alone (pcDNA3) ($n=3$, $P<0.05$). **I** Bar graph showing a decrease in Nanog promoter activity upon siRNA mediated RhoC knockdown (RhoC siR) in comparison with scrambled negative control (SCR) ($n=3$, $P<0.05$). **J** Bar graph depicting the decrease in Nanog promoter activity upon WDR5 silencing (WDR5 siR) in comparison with scrambled control (SCR) ($n=3$, $p<0.05$)

RhoC is co-expressed with stemness genes, Nanog and CD49f, in a sub-population of tumor cells

Our data establish that RhoC regulates the expression of pluripotency genes and hence the maintenance of CSCs. Since both Nanog and CD49f are essential stemness markers [21, 39], we postulated that a cell co-expressing RhoC/Nanog or RhoC/CD49f would putatively be a CSC. Thus studies were performed to identify such a sub-population, using cervical carcinoma cell lines and clinical specimens.

In concordance with the data from cell lines and xenografts, immunofluorescent-based expression analysis of Nanog, CD49f and RhoC in cervical tumor specimens, revealed the existence of a sub-population of cells co-expressing RhoC along with Nanog and CD49f. As shown in Fig. 8A and S6A, pockets of tumor cells that displayed

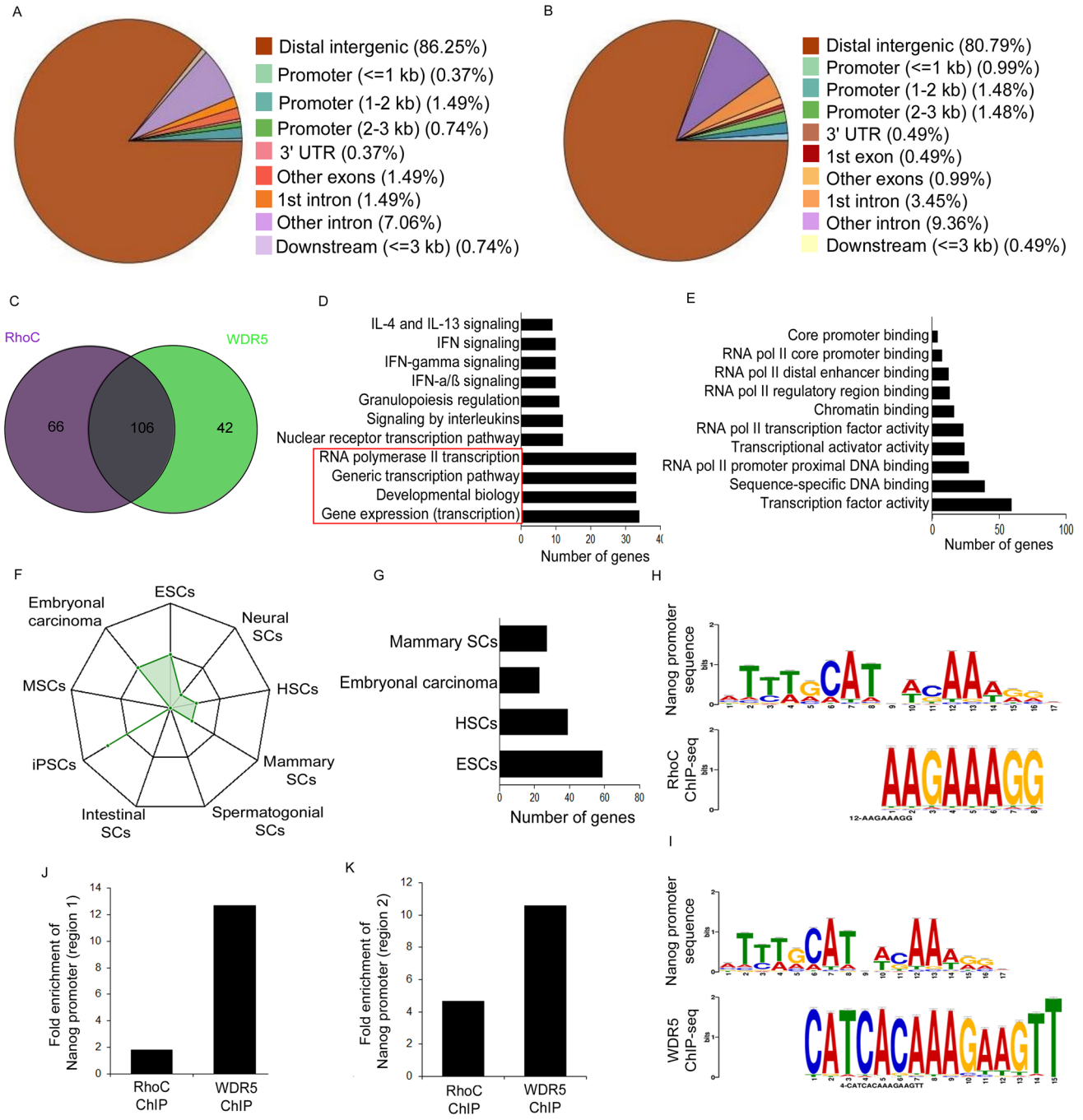

Fig. 7 RhoC and WDR5 bind to identical DNA motifs to transcriptionally regulate pluripotency factors. **A** Pie chart of the genome annotation of the ChIP-seq reads identified by RhoC pull-down. **B** Pie-chart depicting genome annotation of regions of the DNA pulled-down by ChIP-seq using WDR5 antibody. **C** Venn diagram depicting the number of genes occupied by RhoC alone, WDR5 alone and those commonly occupied by both. **D** Bar graph representation of the biological processes governed by the genes commonly occupied by RhoC and WDR5 as identified by the STRING network. **E** Bar graph representation of the molecular functions of genes commonly occupied by RhoC and WDR5. **F** Diagrammatic representation of the stemness signatures enriched by the genes commonly occupied by RhoC and WDR5. **G** Bar graph depicting the number of genes commonly occupied by both RhoC and WDR5 and the stemness phenotypes they enrich for. **H** Diagrammatic representation of the motif in the Nanog promoter found in the RhoC ChIP-seq reads. **I** Diagrammatic representation shows that the identical motif in the Nanog promoter was enriched in the WDR5 ChIP-seq data. **J** and **K** qPCR of the ChIP DNA showing occupation of both halves of the Nanog promoter by RhoC and WDR5, thus validating the ChIP-seq data. Data were normalized against the isotype control ($n=2$)

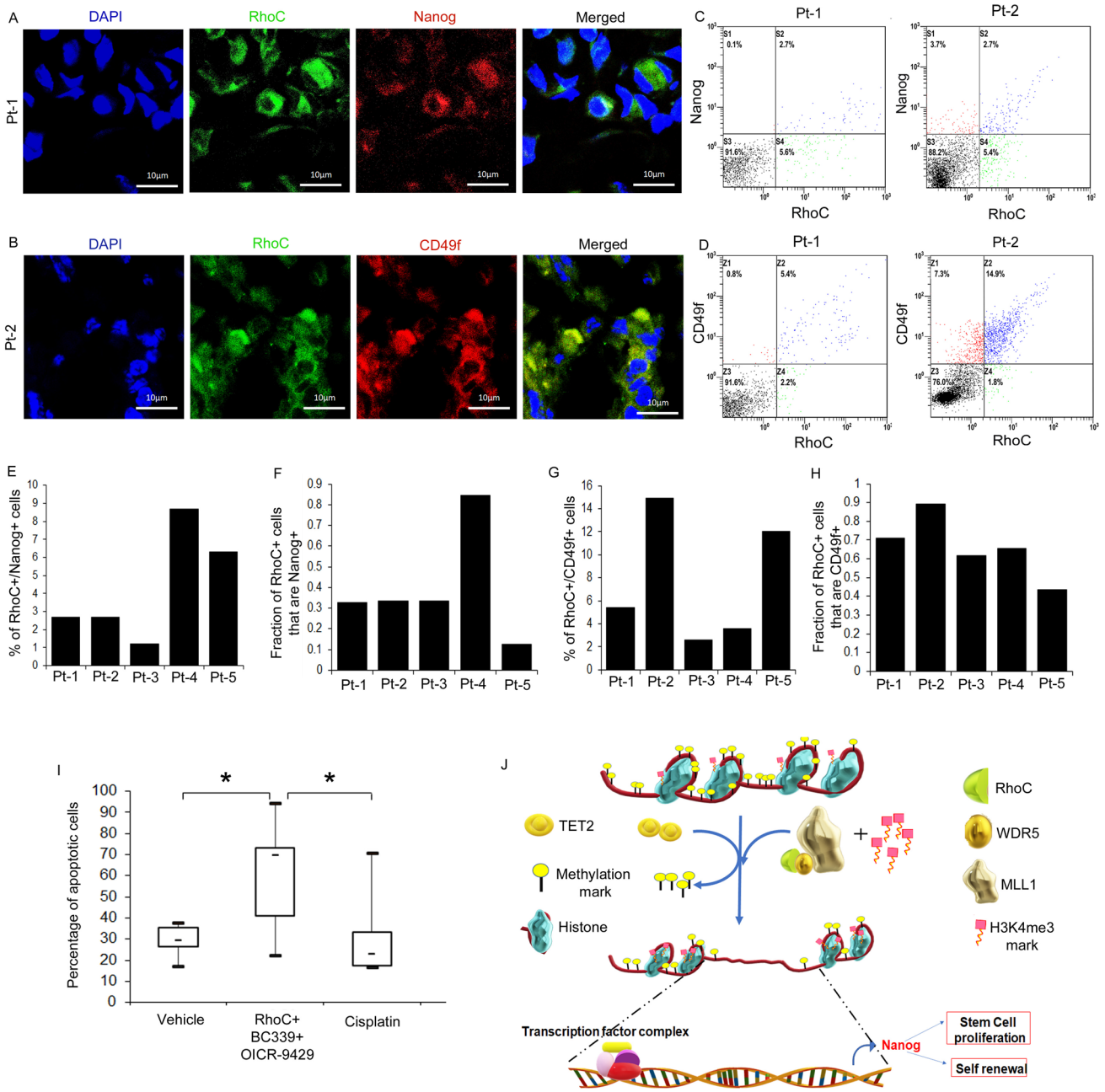

Fig. 8 Biopsy-derived RhoC expressing cells co-express CSC markers Nanog and CD49f, and combinatorial inhibition of RhoC, TET2 and WDR5 sensitize cervical biopsy-derived cells to radiation. **A** Representative immunofluorescent confocal images depicting increased expression of Nanog in RhoC-high tumor cells (scale bars are indicated). **B** Representative immunofluorescent confocal images depicting increased expression of CD49f in RhoC-high tumor cells (scale bars are indicated). **C** FACS quadrant plot showing the distribution of RhoC and Nanog positivity patients Pt-1 and Pt-2. **D** FACS quadrant plot showing the distribution of RhoC and CD49f positivity patients Pt-1 and Pt-2. **E** Bar graph representation of the percentage of dual RhoC$^+$/Nanog$^+$ cells in patients Pt-1 to Pt-5. **F** Graphical representation of the fraction of Nanog positivity within the RhoC$^+$ pool. **G** Bar graph representation of the percentage of dual RhoC$^+$/CD49f$^+$ cells in patients Pt-1 to Pt-5. **H** Graphical representation of the fraction of CD49f positivity within the RhoC$^+$ pool. **I** Box-whisker plot indicating that combined inhibition of RhoC, TET2 and WDR5 led to significant sensitization of cervical cancer biopsy-derived cells to radiation, in comparison with both vehicle control (DMSO + IgG) and cisplatin treatment before radiation ($n = 5$). **J** Model depicting RhoC's two-pronged role in epigenetic regulation of stemness

increased expression of Nanog and RhoC were observed in multiple clinical specimens. Similarly, tumor cells expressing both RhoC and CD49f were detected in these specimens (Fig. 8B and S6B).

A quantitative assessment using flow cytometry confirmed the existence of dually marked, $RhoC^+/Nanog^+$ and $RhoC^+/CD49f^+$ cells. The $RhoC^+/Nanog^+$ cell population ranged from 1.2 to 8.7%, while the $RhoC^+/CD49f^+$ cells comprised between 2.6 and 14.9% of the total cellular pool (Fig. 8C, D, S6C and S6D). Further analysis revealed that a significant percentage of total RhoC cells showed positivity for Nanog (Fig. 8E and F). Similarly, a considerable percentage of the cells showing positivity for RhoC were also $CD49f^+$ (Fig. 8G and H). Investigations using SiHa cells also show the existence of $RhoC^+/Nanog^+/CD49f^+$ (triple positive cells), implying the presence of a CSC population marked by Nanog, CD49f and RhoC (Fig. S6E). Since both Nanog and CD49f are well-established CSC markers, co-expression of RhoC within the pool of cells marked by Nanog and CD49f confirmed the role of RhoC in CSC maintenance.

Combined inhibition of RhoC, TET2 and WDR5 results in sensitization of cervical cancer cells to radiation

Our data thus far comprehensively establishes that RhoC, via TET2 over-expression and WDR5 interaction, results in increased transcription of stemness-associated genes. Since stem-like cells contribute to enhanced survival and resistance to therapy, thus, experiments investigating the role of combined inhibition of RhoC, TET2 and WDR5 in the sensitization of cervical cancer cells to radiation were performed. The antibody inhibition method was used for specific inhibition of RhoC [11]. BC339 and OICR-9429, established chemical inhibitors of TET2 and WDR5 respectively [40, 41], were used at concentrations of 100 µM and 10 µM as determined by WST analysis (Figs. S7A and S7B). Patient-derived biopsies ($n=5$) treated with RhoC antibody, BC339 and OICR-9429, followed by radiation, were compared against concurrent cisplatin and radiation (the current treatment protocol) for sensitization efficiency. The combinatorial inhibition study on clinical samples revealed that the percentage of apoptotic cells was significantly higher upon cumulative inhibition of RhoC, TET2 (BC339) and WDR5 (OICR-9429), with a median Annexin V positivity of 69.8% as compared to the vehicle control ($P<0.05$) (Figs. 8I and S7C). Interestingly, combinatorial treatment of cells with BC339, OICR-9429 and RhoC antibody resulted in a higher percentage of apoptotic cells than that achieved by cisplatin treatment followed by irradiation (median = 22.8%, $P<0.05$) (Fig. 8I).

Overall, this work convincingly portrays the role of RhoC in cervical CSC maintenance and establishes that RhoC epigenetically alters the stemness capability of tumor cells via TET2 and WDR5 (Fig. 8J).

Discussion

The International Agency for Research on Cancer (IARC) released statistics showing an alarming 10 million cancer-related deaths in 2020, with one in every eight men and one in every eleven women succumbing to the disease. Tumor recurrence, resistance and metastasis are crucial factors affecting clinical outcomes and have been closely associated with tumor heterogeneity and CSCs [6, 42, 43]. CSCs demonstrate multiple hallmarks of cancer and cruise through dynamically changing microenvironments during their transit from the primary tumor to secondary sites of metastasis [44]. The molecular profiles of these cells vary distinctly at every stage of tumor progression, and the discovery of novel molecular targets will help in designing effective therapeutic strategies to target CSCs and achieve favorable prognoses [45]. Our earlier study shows that RhoC regulates radio-resistance in cervical cancer via ROCK2 signaling [11]. Reports also suggest that RhoC regulates several other tumor phenotypes in cervical carcinoma, including invasion, anoikis, tumor growth and metastasis [12]. RhoC has similar oncogenic roles in a host of other tumor models [7].

Interestingly, RhoC has no reported driver mutations [46], and is indispensable for metastasis [10]. Since earlier scientific investigations have confirmed the link between CSCs and metastasis [43, 47, 48], the present study explores the role of RhoC in cervical CSC regulation, and reports that RhoC regulates cervical CSCs via interaction with the epigenetic modulator, WDR5.

The three major findings of this study are, (a) RhoC regulates stemness phenotype and expression of stemness-associated genes in cervical cancer, (b) RhoC interacts with WDR5 and MLL1, key components of the SET/COMPASS complex involved in epigenetic regulation, and (c) RhoC promotes DNA demethylation via TET2 expression. Investigations using transcriptomic studies showed that RhoC over-expression results in increased expression of stemness-associated genes in SiHa cells. Colony formation, spheroid formation and anoikis resistance abilities increased upon RhoC over-expression. The tumor sphere and dye exclusion assay confirmed that RhoC expression affects the enrichment of stem cells in SiHa cells. The transcriptional up-regulation of a sizeable portion of the genome (27%) upon over-expression of RhoC suggests that RhoC positively regulates a complex transcriptional network. These observations led us to believe that it may regulate either modifications to histone

proteins or to the DNA itself to effect sweeping changes to the transcriptome.

Several reports suggest that RhoC regulates various signaling pathways, like MAPK, PI3K/Akt, Pyk2 and FAK, in several tumor models [13, 14, 49]. However, its role in epigenetic modifications to the DNA is unknown. In this study, we observed that alterations in the expression of RhoC resulted in changes in the methylation status of the SiHa cell genome. Consistent with our hypothesis, there was enhanced DNA demethylation upon RhoC over-expression and vice versa. TET family genes influence DNA demethylation [50–53]. TET1 regulates stem-like ability in pre-cancerous cervical lesions and drives cancer growth via DNA demethylation in hepatocellular carcinoma [54, 55]. Although we do not observe a significant change in TET1 expression upon changes in the level of RhoC, there was significant up-regulation of TET2 upon RhoC over-expression. Earlier reports suggest that TET2, which marks for slow cycling cells is associated with therapy resistance, while other studies imply a tumor suppressive role for TET2 [56, 57]. We observe that RhoC regulates the expression of TET2 to influence DNA methylation. Infinium array-based study on cells over-expressing RhoC revealed decreased methylation signatures for important genes such as Nanog, Sox2 and ABCG2. However, the mechanism of regulation of TET2 expression by RhoC is not well defined and is the focus of current studies.

It is well-known that RhoC does not have a DNA binding domain. However, its expression in the nuclei of tumor cells has been recently reported by our group in the context of radioresistance [11], indicating that it may be associated with other nuclear proteins to influence transcription. To elucidate its mechanism of action, studies were performed to identify the nuclear binding partners of RhoC. Immunoprecipitation from nuclear lysates, followed by mass spectrometry analysis revealed that WDR5 bound to RhoC. The other protein which was found to associate with RhoC was MLL1. Both WDR5 and MLL1 are major components of the SET1/COMPASS complex involved in histone modifications [32]. It has been shown to regulate therapy resistance in colon cancer, is involved in breast cancer progression [32, 58] and promotes pancreatic, prostate and gastric cancers [59–61]. Observations revealed that the association between WDR5 and RhoC resulted in significant changes in the expression of stemness associated genes, such as Nanog. Nanog is an important pluripotent gene, and its expression correlates with the stemness status of the cell [62, 63]. Our reporter assays and ChIP-seq assay confirm that RhoC and WDR5 regulate the expression of Nanog in SiHa cells. Motif analysis of genes identified by RhoC ChIP-seq reveals enrichment of stemness-associated genes. Interestingly, the motifs enriched by WDR5 and RhoC were the same. This is a novel observation, as no previous literature suggests an interaction between RhoC and WDR5 in the context of epigenetic events.

In the context of our observations that RhoC expression regulates radiation response, stemness phenotype and cell survival, it is interesting to note our finding that inhibition of RhoC, TET2 and WDR5 in human specimen-derived cells results in enhanced sensitization to radiation. The sensitization was significantly more than the cisplatin-based sensitization of these cells. Further, analysis of heterogeneity of cell populations, based on RhoC and Nanog expression revealed the existence of a small population of tumor cells co-expressing both RhoC and Nanog. Similarly, a subpopulation was identified with co-expression of RhoC and CD49f. Since Nanog and CD49f mark for CSCs, it is interesting to note that RhoC is co-expressed with these proteins.

Thus, combined, these findings provide an intensive analysis of RhoC-mediated regulation of stemness-associated gene expression and associated phenotypes, and identify WDR5 as its associate in this context. These findings provide a robust basis for understanding RhoC-mediated maintenance of CSCs in cervical carcinoma. Despite a thrust on identifying biomarkers for cancers, there is lacking in the field of cervical carcinoma. We have previously reported that RhoC over-expression correlates with tumor progression [11, 12], wherein there was increased expression of RhoC in cervical carcinoma samples compared to normal tissues. This observation, combined with our recent findings that RhoC regulates therapy response and CSC maintenance in cervical carcinoma, positions RhoC as a strong biomarker candidate for this tumor. We have also investigated if RhoC over-expression regulated stemness gene expression and associated phenotypes in other tumor models, and we observed a similar phenomenon in PC-3 and HCT 116 cells (Fig. S8).

This study defines a new role for RhoC as a regulator of the transcriptional network via its interaction with the epigenetic complex and supports the development of RhoC as a biomarker of disease progression and therapeutic intervention.

Supplementary Information The online version contains supplementary material available at https://doi.org/10.1007/s00018-022-04645-z.

Acknowledgements We would like to thank the Department of Science and Technology (DST), India for funding. Pavana Thomas has been awarded a fellowship by the Council for Scientific and Industrial Research (CSIR), India for the course of her PhD. Dr Sweta Srivastava was awarded a travel grant by the Indian Council for Medical Research (ICMR). We would like to thank the Central Imaging and Flow Facility (CIFF) at National Centre for Biological Sciences (NCBS), Bangalore for help with selected flow experiments.

Author contributions PT: concept and design, data acquisition, analysis and interpretation, drafting of the manuscript, final approval. SS: concept and design, data acquisition, analysis and interpretation, drafting of the manuscript, final approval. AHU: sample collection and

clinical data analysis, revision of the manuscript, final approval. SD: data acquisition, analysis. LY: data acquisition, analysis. BM: acquisition and interpretation of 2D gel data, final approval. SBS: acquisition and analysis of flow cytometry data. AKM: acquisition and interpretation of 2D gel data. NS: sample collection and clinical data acquisition. All authors have read and approved the final manuscript.

Availability of data and material The datasets during and/or analyzed during the current study are available on Annotare 2.0.

Declarations

Conflict of interest The authors declare that they have no competing interests.

Ethical approval and consent to participate The study was approved by the Institutional Ethics Committee (IEC) at St. John's Medical College. The samples were collected with patient consent and all experiments were carried out as per the guidelines.

Consent for publication Not applicable.

References

1. Sung H, Ferlay J, Siegel RL, Laversanne M, Soerjomataram I, Jemal A, Bray F (2021) Global Cancer Statistics 2020: GLOBOCAN estimates of incidence and mortality worldwide for 36 cancers in 185 countries. CA Cancer J Clin 71(3):209–249
2. Endo D, Todo Y, Okamoto K, Minobe S, Kato H, Nishiyama N (2014) Prognostic factors for patients with cervical cancer treated with concurrent chemoradiotherapy: a retrospective analysis in a Japanese cohort. J Gynecol Oncol 26(1):12–18
3. Kim TE, Park BJ, Kwack HS, Kwon JY, Kim JH, Yoon SC (2012) Outcomes and prognostic factors of cervical cancer after concurrent chemoradiation. J Obstet Gynaecol Res 38(11):1315–1320
4. Steinbichler TB, Dudas J, Skvortsov S, Ganswindt U, Riechelmann H, Skvortsova II (2018) Therapy resistance mediated by cancer stem cells. Semin Cancer Biol 53:156–167
5. Chang JC (2016) Cancer stem cells: Role in tumor growth, recurrence, metastasis, and treatment resistance. Medicine (Baltimore) 95(1 Suppl 1):S20–S25
6. Najafi M, Mortezaee K, Majidpoor J (2019) Cancer stem cell (CSC) resistance drivers. Life Sci 234:116781
7. Thomas P, Pranatharthi A, Ross C, Srivastava S (2019) RhoC: a fascinating journey from a cytoskeletal organizer to a cancer stem cell therapeutic target. J Exp Clin Cancer Res 38(1):328
8. Chardin P, Boquet P, Madaule P, Popoff MR, Rubin EJ, Gill DM (1989) The mammalian G protein rhoC is ADP-ribosylated by Clostridium botulinum exoenzyme C3 and affects actin microfilaments in Vero cells. EMBO J 8(4):1087–1092
9. Clark EA, Golub TR, Lander ES, Hynes RO (2000) Genomic analysis of metastasis reveals an essential role for RhoC. Nature 406(6795):532–535
10. Hakem A, Sanchez-Sweatman O, You-Ten A, Duncan G, Wakeham A, Khokha R, Mak TW (2005) RhoC is dispensable for embryogenesis and tumor initiation but essential for metastasis. Genes Dev 19(17):1974–1979
11. Pranatharthi A, Thomas P, Udayashankar AH, Bhavani C, Suresh SB, Krishna S, Thatte J, Srikantia N, Ross CR, Srivastava S (2019) RhoC regulates radioresistance via crosstalk of ROCK2 with the DNA repair machinery in cervical cancer. J Exp Clin Cancer Res 38(1):392
12. Srivastava S, Ramdass B, Nagarajan S, Rehman M, Mukherjee G, Krishna S (2009) Notch1 regulates the functional contribution of RhoC to cervical carcinoma progression. Br J Cancer 102(1):196–205
13. Ruth MC, Xu Y, Maxwell IH, Ahn NG, Norris DA, Shellman YG (2006) RhoC promotes human melanoma invasion in a PI3K/Akt-dependent pathway. J Invest Dermatol 126(4):862–868
14. van Golen KL, Bao LW, Pan Q, Miller FR, Wu ZF, Merajver SD (2002) Mitogen activated protein kinase pathway is involved in RhoC GTPase induced motility, invasion and angiogenesis in inflammatory breast cancer. Clin Exp Metastasis 19(4):301–311
15. van Golen KL, Wu ZF, Qiao XT, Bao L, Merajver SD (2000) RhoC GTPase overexpression modulates induction of angiogenic factors in breast cells. Neoplasia 2(5):418–425
16. Zhao ZH, Tian Y, Yang JP, Zhou J, Chen KS (2015) RhoC, vascular endothelial growth factor and microvascular density in esophageal squamous cell carcinoma. World J Gastroenterol 21(3):905–912
17. Islam M, Sharma S, Teknos TN (2014) RhoC regulates cancer stem cells in head and neck squamous cell carcinoma by overexpressing IL-6 and phosphorylation of STAT3. PLoS ONE 9(2):e88527
18. Rosenthal DT, Zhang J, Bao L, Zhu L, Wu Z, Toy K, Kleer CG, Merajver SD (2012) RhoC impacts the metastatic potential and abundance of breast cancer stem cells. PLoS ONE 7(7):e40979
19. Grimberg J, Nawoschik S, Belluscio L, McKee R, Turck A, Eisenberg A (1989) A simple and efficient non-organic procedure for the isolation of genomic DNA from blood. Nucleic Acids Res 17(20):8390
20. Bailey TL, Johnson J, Grant CE, Noble WS (2015) The MEME suite. Nucleic Acids Res 43(W1):W39-49
21. Lopez J, Poitevin A, Mendoza-Martinez V, Perez-Plasencia C, Garcia-Carranca A (2012) Cancer-initiating cells derived from established cervical cell lines exhibit stem-cell markers and increased radioresistance. BMC Cancer 12:48
22. Hirschmann-Jax C, Foster AE, Wulf GG, Nuchtern JG, Jax TW, Gobel U, Goodell MA, Brenner MK (2004) A distinct "side population" of cells with high drug efflux capacity in human tumor cells. Proc Natl Acad Sci U S A 101(39):14228–14233
23. Lee CH, Yu CC, Wang BY, Chang WW (2015) Tumorsphere as an effective in vitro platform for screening anti-cancer stem cell drugs. Oncotarget 7(2):1215–1226
24. Sieburg HB, Cho RH, Muller-Sieburg CE (2002) Limiting dilution analysis for estimating the frequency of hematopoietic stem cells: uncertainty and significance. Exp Hematol 30(12):1436–1443
25. Lim DA (2015) Transcriptional and epigenetic insights from stem cells and developing tissues. Development 142(15):2549–2553
26. Gaspar-Maia A, Alajem A, Meshorer E, Ramalho-Santos M (2011) Open chromatin in pluripotency and reprogramming. Nat Rev Mol Cell Biol 12(1):36–47
27. Hardy K, Wu F, Tu W, Zafar A, Boulding T, McCuaig R, Sutton CR, Theodoratos A, Rao S (2016) Identification of chromatin accessibility domains in human breast cancer stem cells. Nucleus 7(1):50–67
28. Linhoff MW, Garg SK, Mandel G (2015) A high-resolution imaging approach to investigate chromatin architecture in complex tissues. Cell 163(1):246–255
29. Fraga MF, Herranz M, Espada J, Ballestar E, Paz MF, Ropero S, Erkek E, Bozdogan O, Peinado H, Niveleau A et al (2004) A mouse skin multistage carcinogenesis model reflects the aberrant DNA methylation patterns of human tumors. Cancer Res 64(16):5527–5534
30. Kamdar S, Isserlin R, Van der Kwast T, Zlotta AR, Bader GD, Fleshner NE, Bapat B (2019) Exploring targets of TET2-mediated methylation reprogramming as potential discriminators of prostate cancer progression. Clin Epigenetics 11(1):54

31. Dunn KW, Kamocka MM, McDonald JH (2011) A practical guide to evaluating colocalization in biological microscopy. Am J Physiol Cell Physiol 300(4):C723-742
32. Punzi S, Balestrieri C, D'Alesio C, Bossi D, Dellino GI, Gatti E, Pruneri G, Criscitiello C, Lovati G, Meliksetyan M et al (2019) WDR5 inhibition halts metastasis dissemination by repressing the mesenchymal phenotype of breast cancer cells. Breast Cancer Res 21(1):123
33. Chen X, Xie W, Gu P, Cai Q, Wang B, Xie Y, Dong W, He W, Zhong G, Lin T et al (2015) Upregulated WDR5 promotes proliferation, self-renewal and chemoresistance in bladder cancer via mediating H3K4 trimethylation. Sci Rep 5:8293
34. Bailey TL (2021) STREME: accurate and versatile sequence motif discovery. Bioinformatics 37:2834–2840
35. Tanaka E, Bailey T, Grant CE, Noble WS, Keich U (2011) Improved similarity scores for comparing motifs. Bioinformatics 27(12):1603–1609
36. Heberle H, Meirelles GV, da Silva FR, Telles GP, Minghim R (2015) InteractiVenn: a web-based tool for the analysis of sets through Venn diagrams. BMC Bioinformatics 16:169
37. Jassal B, Matthews L, Viteri G, Gong C, Lorente P, Fabregat A, Sidiropoulos K, Cook J, Gillespie M, Haw R et al (2020) The reactome pathway knowledgebase. Nucleic Acids Res 48(D1):D498–D503
38. Pinto JP, Kalathur RK, Oliveira DV, Barata T, Machado RS, Machado S, Pacheco-Leyva I, Duarte I, Futschik ME (2015) StemChecker: a web-based tool to discover and explore stemness signatures in gene sets. Nucleic Acids Res 43(W1):W72-77
39. Hu J, Liu J, Chen A, Lyu J, Ai G, Zeng Q, Sun Y, Chen C, Wang J, Qiu J et al (2016) Ino80 promotes cervical cancer tumorigenesis by activating Nanog expression. Oncotarget 7(44):72250–72262
40. Zhang X, Yang J, Shi D, Cao Z (2020) TET2 suppresses nasopharyngeal carcinoma progression by inhibiting glycolysis metabolism. Cancer Cell Int 20:363
41. Zhang J, Zhou Q, Xie K, Cheng L, Peng S, Xie R, Liu L, Zhang Y, Dong W, Han J et al (2021) Targeting WD repeat domain 5 enhances chemosensitivity and inhibits proliferation and programmed death-ligand 1 expression in bladder cancer. J Exp Clin Cancer Res 40(1):203
42. Rycaj K, Tang DG (2014) Cancer stem cells and radioresistance. Int J Radiat Biol 90(8):615–621
43. Shiozawa Y, Nie B, Pienta KJ, Morgan TM, Taichman RS (2013) Cancer stem cells and their role in metastasis. Pharmacol Ther 138(2):285–293
44. Yoshida GJ, Saya H (2021) Molecular pathology underlying the robustness of cancer stem cells. Regen Ther 17:38–50
45. Turajlic S, Swanton C (2016) Metastasis as an evolutionary process. Science 352(6282):169–175
46. Alan JK, Lundquist EA (2013) Mutationally activated Rho GTPases in cancer. Small GTPases 4(3):159–163
47. Baccelli I, Trumpp A (2012) The evolving concept of cancer and metastasis stem cells. J Cell Biol 198(3):281–293
48. Pattabiraman DR, Weinberg RA (2014) Tackling the cancer stem cells - what challenges do they pose? Nat Rev Drug Discov 13(7):497–512
49. Iiizumi M, Bandyopadhyay S, Pai SK, Watabe M, Hirota S, Hosobe S, Tsukada T, Miura K, Saito K, Furuta E et al (2008) RhoC promotes metastasis via activation of the Pyk2 pathway in prostate cancer. Cancer Res 68(18):7613–7620
50. Ross SE, Bogdanovic O (2019) TET enzymes, DNA demethylation and pluripotency. Biochem Soc Trans 47(3):875–885
51. Kohli RM, Zhang Y (2013) TET enzymes, TDG and the dynamics of DNA demethylation. Nature 502(7472):472–479
52. Rasmussen KD, Helin K (2016) Role of TET enzymes in DNA methylation, development, and cancer. Genes Dev 30(7):733–750
53. Wu X, Zhang Y (2017) TET-mediated active DNA demethylation: mechanism, function and beyond. Nat Rev Genet 18(9):517–534
54. Su PH, Hsu YW, Huang RL, Chen LY, Chao TK, Liao CC, Chen CW, Wu TI, Mao SP, Balch C et al (2019) TET1 promotes 5hmC-dependent stemness, and inhibits a 5hmC-independent epithelial-mesenchymal transition, in cervical precancerous lesions. Cancer Lett 450:53–62
55. Shirai K, Nagae G, Seki M, Kudo Y, Kamio A, Hayashi A, Okabe A, Ota S, Tsutsumi S, Fujita T et al (2021) TET1 upregulation drives cancer cell growth through aberrant enhancer hydroxymethylation of HMGA2 in hepatocellular carcinoma. Cancer Sci 112(7):2855–2869
56. Zhang T, Cooper S, Brockdorff N (2015) The interplay of histone modifications - writers that read. EMBO Rep 16(11):1467–1481
57. Xu YP, Lv L, Liu Y, Smith MD, Li WC, Tan XM, Cheng M, Li Z, Bovino M, Aube J et al (2019) Tumor suppressor TET2 promotes cancer immunity and immunotherapy efficacy. J Clin Invest 129(10):4316–4331
58. Neilsen BK, Chakraborty B, McCall JL, Frodyma DE, Sleightholm RL, Fisher KW, Lewis RE (2018) WDR5 supports colon cancer cells by promoting methylation of H3K4 and suppressing DNA damage. BMC Cancer 18(1):673
59. Lu C, Liu Z, Klement JD, Yang D, Merting AD, Poschel D, Albers T, Waller JL, Shi H, Liu K (2021) WDR5-H3K4me3 epigenetic axis regulates OPN expression to compensate PD-L1 function to promote pancreatic cancer immune escape. J Immunother Cancer 9(7):e002624
60. Zhou Q, Chen X, He H, Peng S, Zhang Y, Zhang J, Cheng L, Liu S, Huang M, Xie R et al (2021) WD repeat domain 5 promotes chemoresistance and Programmed Death-Ligand 1 expression in prostate cancer. Theranostics 11(10):4809–4824
61. Sun W, Guo F, Liu M (2018) Up-regulated WDR5 promotes gastric cancer formation by induced cyclin D1 expression. J Cell Biochem 119(4):3304–3316
62. Pan G, Thomson JA (2007) Nanog and transcriptional networks in embryonic stem cell pluripotency. Cell Res 17(1):42–49
63. Fatma H, Siddique HR, Maurya SK (2021) The multiple faces of NANOG in cancer: a therapeutic target to chemosensitize therapy-resistant cancers. Epigenomics 13(23):1885–1900

Publisher's Note Springer Nature remains neutral with regard to jurisdictional claims in published maps and institutional affiliations.

Springer Nature or its licensor (e.g. a society or other partner) holds exclusive rights to this article under a publishing agreement with the author(s) or other rightsholder(s); author self-archiving of the accepted manuscript version of this article is solely governed by the terms of such publishing agreement and applicable law.